T-follicular helper cells are epigenetically poised to transdifferentiate into T-regulatory type-1 cells

Josep Garnica[1], Patricia Solé[1], Jun Yamanouchi[2], Joel Moro[1], Debajyoti Mondal[2], Cesar Fándos[1], Pau Serra[1], Pere Santamaria[1,2*]

[1] Institut D'Investigacions Biomèdiques August Pi i Sunyer, Barcelona, 08036, Spain

[2] Department of Microbiology, Immunology and Infectious Diseases, Snyder Institute for Chronic Diseases, Cumming School of Medicine, University of Calgary, Alberta, T2N 4N1 Canada

Correspondence: P. Santamaria (psantama@ucalgary.ca)

Running Title: TFH cells are epigenetically poised to become TR1 cells

Abstract

Chronic antigenic stimulation can trigger the formation of IL-10-producing T-regulatory type 1 (TR1) cells *in vivo*. We have recently shown that T follicular helper (TFH) cells are precursors of TR1 cells and that the TFH-to-TR1 cell transdifferentiation process is characterized by the progressive loss and acquisition of opposing transcription factor gene expression programs that evolve through at least one transitional cell stage. Here, we use a broad range of bulk and single-cell transcriptional and epigenetic tools to investigate the epigenetic underpinnings of this process. At the single cell level, the TFH-to-TR1 cell transition is accompanied by both, downregulation of TFH cell-specific gene expression due to loss of chromatin accessibility, and upregulation of TR1 cell-specific genes linked to chromatin regions that remain accessible throughout the transdifferentiation process, with minimal generation of new open chromatin regions. By interrogating the epigenetic status of accessible TR1 genes on purified TFH and conventional T cells, we find that most of these genes, including *Il10*, are already poised for expression at the TFH cell stage. Whereas these genes are closed and hypermethylated in Tconv cells, they are accessible, hypomethylated and enriched for H3K27ac-marked and hypomethylated active enhancers in TFH cells. These enhancers are enriched for binding sites for the TFH and TR1-associated transcription factors TOX-2, IRF4 and c-MAF. Together, these data suggest that the TR1 gene expression program is genetically imprinted at the TFH cell stage.

Introduction

Interleukin 10 (IL-10)-producing regulatory T-cells (Tregs) play a central role in the maintenance of normal immune homeostasis. Treg cells include the well-characterized FOXP3$^+$ subset as well as a FOXP3-negative CD4+ T-cell type that secretes IL-10 and low levels or no IL-4 and co-expresses CD49b, LAG-3, Inducible T-cell costimulator (ICOS) and/or CCR5 and PD-1 among others (1).

We have shown that systemic delivery of nanoparticles (NPs) coated with mono-specific peptide-major histocompatibility complex class II (pMHCII) molecules (2) triggers the expansion and re-programming of cognate splenic T-Follicular helper (TFH) CD4$^+$ T-cells into expanded pools of transitional (referred to as TR1.1 or TR1-like) and terminally differentiated TR1 cells (referred to as TR1.2 or TR1) that resolve inflammation in various organ-specific autoimmune disease models in a disease-specific manner without impairing normal immunity (3-5). These events result from the sustained assembly of large TCR microclusters, and rapid, robust and prolonged TCR signaling on TFH cells (2, 6, 7). The antigen-specific TFH and TR1 sub-pools arising in response to pMHCII-NP therapy have nearly identical clonotypic composition but alternative functional properties and transcription factor expression profiles (6). In addition, pMHCII-NPs trigger cognate TR1 cell formation in TFH cell-transfused immunodeficient hosts, and T-cell-specific deletion of two master regulators of TFH cell genesis (*Bcl6* or *Irf4*) blunt both pMHCII-NP-induced TFH expansion and TR1 formation. In contrast, deletion of *Prdm1* selectively abrogates the TFH-to-TR1 conversion. Together, these data indicated that TFH cells can differentiate into TR1 cells *in vivo* and that Blimp-1 is a gatekeeper of this cell re-programming event (6). The work described herein was initiated to test the hypothesis that pMHCII-NP-induced conversion of TFH cells into TR1 cells involves epigenetic re-programming of the TFH precursors.

Chromatin can be modified at various levels, including alterations in chromatin accessibility to expose or shield specific genes from the gene expression machinery, through

histone modifications that either promote or repress gene expression, or via changes in DNA methylation, typically hypomethylation. Although such processes have been shown to contribute to T cell differentiation, such as during Th1/Th2 cell specification (8), they can also occur upon T-cell activation (9) or in response to environmental cues, such as cytokine stimulation (10). Likewise, it has been established that DNA methylation, histone modifications and chromatin accessibility regulate T cell activation and effector and memory responses during immune responses to infection. Effector T cell-specific genes are demethylated and gain chromatin accessibility and naïve T cell-associated genes are repressed. When these cells need to become memory, the naïve genes required for survival are demethylated (11). Another notable example of chromatin remodeling is in exhausted T cells, where numerous effector genes, such as *Ifng*, become closed, and acquire open chromatin at genes that are upregulated in these cells, such as *Pdcd1* (11).

Several notable examples of redistribution of histone marks during T cell differentiation have been described. For example, Th1 differentiation results in H3K4 di-methylation and H3 and H4 acetylation and in the creation of chromatin accessible regions at regulatory elements within the *Ifng* locus, as well as in the loss of H3K27me3 through the locus (in addition to DNA demethylation of the locus) (12, 13). In contrast, activation of the Th2 program leads to the loss of permissive histone modifications in *Ifng*, addition of repressive H3K27me3 marks along the locus and DNA methylation (13-15). Th2 differentiation from naïve precursors also involves the acquisition of permissive histone modifications in *Il4, Il5, Il13* and the locus control region (LCR), and the loss of H3K27me3 marks (9, 16). Likewise, the promoters and eight gene regulatory elements of *Il17a* and *Il17f* genes in naïve CD4+ T cells acquire H3K27ac marks upon culture in Th17-polarising conditions (17). In memory T cells, which display faster and greater levels of gene transcription than their naïve and effector counterparts, lineage-specific cytokine genes retain the positive histone modifications on their proximal and distal gene regulatory elements that were acquired during differentiation of their precursor T cells (e.g. H3K27ac and H3K9ac marks), even

when expression of the genes ceases upon memory cell conversion, allowing rapid reactivation of these loci upon antigen re-encounter (18). Likewise, naive CD8+ T cells lose repressive H3K27me3 marks during the primary immune response against infections, allowing rapid upregulation of *Ifng* and *Gzmb* expression by their memory CD8+ T cell counterparts (19). Overall, memory T cells appear to retain the epigenetic signatures of their effector progenitors, thus allowing a quicker and more efficient response in subsequent antigen encounters.

There are also several noteworthy examples of changes in DNA methylation in T cells. For example, the *Cd4* locus is hypermethylated in CD4–CD8–, CD4+CD8+ thymocytes and mature CD8+ T cells, but is demethylated in CD4+CD8– cells (20). Likewise, in naïve T cells, *Il4, Il5, Il13* and the corresponding LCR are hypermethylated and *Ifng* is hypomethylated (21, 22). Whereas this methylation pattern is maintained during the Th0-Th1 differentiation process, it undergoes dramatic changes during Th2 formation, such that *Ifng* becomes hypermethylated, and *Il4, Il5, Il13* and the LCR demethylate key gene regulatory elements (21-23), in addition to acquiring the type of permissive histone modifications discussed above (9, 16). Likewise, TFH formation from naïve T cell precursors involves demethylation of BCL-6 binding sites (24). In Foxp3+ Treg cells, the expression of *Foxp3* and genes coding for some Treg-function associated molecules, such as *Ctla4* and *Il2ra*, but not genes coding for transcription factors controlling other cell fates or cytokine genes that are repressed in Foxp3+ Treg cells, are also associated with DNA demethylation (25, 26). The development of memory T cells also involves progressive demethylation of promoter-distal gene regulatory elements of key genes (27).

Collectively, the above observations indicate that, in most cases, acquisition of new functional states by peripheral T cells, including their differentiation into different T cell subsets involves extensive and diverse modifications of the chromatin around specific loci, although global (i.e. genome-wide) epigenetic changes during these processes were not always explored. Here we show, through a broad combination of transcriptomic and epigenetic studies, that the TFH-to-TR1 transdifferentiation process does not follow this pattern. Specifically, we find that

conventional TFH cells are epigenetically poised to differentiate into TR1 cells, and that the TFH-to-TR1 transdifferentiation process is associated with extensive contraction of the chromatin and the upregulation of genes that are already epigenetically poised for expression, yet are silent, at the TFH cell stage, such as *Il10*. These genes are closed and hypermethylated in Tconv cells, but are accessible, hypomethylated and enriched for H3K27ac-marked and hypomethylated active enhancers in TFH cells. These data suggest that genomic imprinting is a key enabler of the TFH-TR1 cell transdifferentiation process, as documented in non-immune cell types (28-30).

Results

Single-cell multiomic profiles of pMHCII-NP-induced TFH and TR1 cells

The compaction status of the chromatin has a direct impact on gene expression, by modulating the accessibility of transcription factor binding sites and the physical interactions between gene regulatory elements (GREs). We therefore sought to map changes in the genome-wide distribution and location of open chromatin regions (OCRs) along the TFH-TR1 pathway and determine whether pMHCII-NP-induced TR1-like cells inherit their chromatin exposure status from TFH cell precursors. We focused on the BDC2.5mi/I-A^{g7} Tet+ cells arising in BDC2.5mi/I-A^{g7}-NP-treated nonobese diabetic (NOD) mice. BDC2.5mi/I-A^{g7}-specific CD4+ T cells comprise a population of autoreactive T cells that contribute to the progression of spontaneous autoimmune diabetes in NOD mice. The size of this type 1 diabetes-relevant T cell specificity is small and barely detectable in untreated NOD mice, but treatment with cognate pMHCII-NPs leads to the expansion and formation of anti-diabetogenic TR1 cells that retain the antigenic specificity of their precursors (3). As a result, treatment of hyperglycemic NOD mice with these compounds results in the reversal of type 1 diabetes (3).

Since the pMHCII-NP-induced Tet+ cell pools contain TFH and TR1 sub-pools (~30% and 70%, respectively) (6, 7), we addressed this question by analyzing the single-cell Multiome (scATACseq + scRNAseq) profiles of BDC2.5mi/I-A^{g7}-NP-induced Tet+ cells. Whereas scRNAseq provides information about the transcriptional identity of the various cellular sub-pools, scATACseq (Assay for Transposable-Accessible Chromatin using sequencing) reveals locations of accessible chromatin at regulatory and non-regulatory regions (31) at each cell differentiation stage along the TFH-TR1 pathway. Furthermore, to ascertain whether the pMHCII-NP-induced Tet+ TFH cells and conventional (i.e. vaccine-induced) TFH cells are equivalent not only at the transcriptional level but also at the level of chromatin accessibility, we also compared the scMultiome profiles of pMHCII-NP-induced Tet+ cells with those corresponding to: 1) purified

Keyhole Limped Hemocyanin (KLH)-induced TFH ($CD4^+CD44^+CXCR5^{high}PD1^{high}$) cells from immunized NOD mice, which are transcriptionally identical to the Tet+ TFH cell pools from BDC2.5mi/I-A^{g7}-NP-treated NOD mice (6, 7); and 2) TH0 ($CD4^+CD44^-CXCR5^-PD1^-$) (naïve) cells obtained from KLH-immunized animals as a control, herein referred to as Tconv cells. We note that studies of Tet+ T cell pools before and after treatment are not possible as the frequency of Tet+ cells in the absence of treatment is below the level of detection via flow cytometry.

Cell clustering using the pMHCII-NP-induced Tet+ cell pool's two-dimensional scRNAseq and scATACseq dataset analysis using Weighted Nearest Neighbor (WNN) revealed the presence of a well-defined TFH-like cell cluster and a larger cluster of cells containing both TR1-like and TR1 cells (6). The KLH-induced TFH subset contained 3 subpools of TFH cells that we referred as TFH.1, TFH.2 and TFH.3 (**Fig. 1A**). The scMultiome profile of the BDC2.5mi/I-A^{g7}-NP-induced TFH cell sub-pool overlapped with the KLH-induced TFH1.1 sub-pool, corresponding to effector *Bcl6*^{hi}*Tox2*^{hi}*Il21*$^+$*Pdcd1*$^+$ TFH cells (**Fig. 1A, left**). At the scRNAseq level, the KLH-induced TFH.2 cells were also similar to their TFH.1 counterparts but expressed lower levels of *Pdcd1, Il21, Bcl6* and *Tox2* and higher levels of *Maf, Tcf7, Cxcr5* and *Cd69* (6). In contrast, the KLH-induced TFH.3 cells display transcriptomic features of Follicular T-regulatory (FTR) cells (*Foxp3*$^+$*Bcl6*$^+$*Bhlhe40*$^+$*Icos*$^+$*Il10*$^+$) (6).

Further mono-omic analyses of the scRNAseq and scATACseq data of the scMultiome datasets provided additional information on the lineage relationships among the various T cell sub-pools. Specifically, UMAP dimensional reduction of the scRNAseq data confirmed a high degree of transcriptional similarity between the TFH.1 cells from the KLH-induced TFH cell pool and the TFH-like cells contained within the BDC2.5mi/I-A^{g7}-NP-induced Tet+ pool (**Fig. 1A, middle**). In fact, these two highly similar subsets only had 5 differentially expressed genes ($|log2FC| > 0.5$ and adjusted $P<0.05$; *Actb, Ifi27l2a, Inpp4b, Nav2* and *Tmsb10*) (**Suppl. Fig. 1**). Dimensional reduction of the scATACseq data showed that the open chromatin landscapes of the

KLH-induced TFH.1 and TFH.2 subpools co-localized with those corresponding to the BDC2.5mi/I-A^{g7}-NP-induced Tet+ TFH and TR1 sub-pools (**Fig. 1A, right**).

The transcriptional and epigenetic relationships among these various T-cell subsets were confirmed by hierarchical clustering of the two-dimensional scMultiome datasets (**Fig. 1B**); despite coming from different mice and arising in response to different cues, the BDC2.5mi/I-A^{g7}-NP-induced TFH cells and the KLH-induced TFH.1/TFH.2 cells were more similar to each other than to other cell subsets within each sample.

Extensive closure of open chromatin during the TFH-to-TR1 cell conversion within the Tet+ cell pool

Comparison of the scATACseq profiles of the KLH-induced TFH and BDC2.5mi/I-A^{g7}-NP-induced Tet+ TFH subpools indicated that TFH cells undergo massive closure of open chromatin regions as they transdifferentiate into TR1-like and TR1 cells (**Fig. 1C**). The data further indicated that most, albeit not all, of the open chromatin regions that remain open in the terminally differentiated TR1 subset and, especially, the transitional TR1-like cells were already open at the TFH.1 cell stage (**Fig. 1C**). Thus, the TFH-to-TR1 cell conversion process involves massive contraction of the chromatin and limited generation of new OCRs.

Chromatin closure during the TFH-to-TR1 conversion within the Tet+ pool is associated with massive silencing of gene expression

Binding of transcription factors to their corresponding binding sites in DNA (TFBS) typically occurs in nucleosome-free regions in open chromatin. We next used the scMultiome datasets to investigate the effects of chromatin remodeling on gene expression during the TFH-to-TR1 cell conversion at the single-cell level. We focused on differentially open chromatin regions in BDC2.5mi/I-A^{g7}-NP-induced TR1-like/TR1 cells (including both the TR1-like and TR1 sub-clusters) or TFH.1 cells (including both the BDC2.5mi/I-A^{g7}-NP-induced TFH and the KLH-induced

TFH.1 cluster) as compared to their Tconv counterparts. We identified 688 genes that were associated with chromatin regions specifically open in TFH cells but not TR1-like/TR1 cells, and 545 genes that were associated with chromatin regions open in both TFH and TR1like/TR1 cells or only TR1-like/TR1 cells.

Analyses of the scRNAseq data from the scMultiome dataset confirmed that chromatin closure during the TFH to TR1 cell conversion was accompanied by an equally extensive downregulation of gene expression. Specifically, there were 2,086 genes that were differentially expressed in TR1 vs. TFH cells. Among these 2,086 genes, 1,820 (87.2%) were downregulated (e.g., *Cxcr5, Il4, Bcl6, Nfia, Stat4, Tcf7* and *Tox2)* and only 266 (12.8%) were upregulated (e.g. *Bach2, Cd226, Ccr5, Ifng, Il10, Lef1, Prdm1* and *Tbx21*) (**Fig. 1D**).

Further analyses focusing on the genes that had closed chromatin regions during the TFH-to-TR1 conversion, confirmed that there was a highly significant association between chromatin closure and downregulation of gene expression between TR1 and TFH cells. Specifically, 94% (n=217/231) of the genes associated with chromatin regions that had closed during the TFH-TR1 conversion, but only 31% (n=4/13) of the newly acquired OCRs, were downregulated (the remaining 69% were upregulated) (P = 8.25e-14) (**Fig. 1E**). Thus, massive chromatin closure during the TFH to TR1 conversion is accompanied by significant gene downregulation.

In contrast, the relative frequency of upregulated and downregulated genes among those linked to the 1,245 regions equally accessible in TR1 and TFH cells (n=196), was similar to that seen for global gene expression changes during the TFH-to-TR1 conversion (86.7% genes downregulated) (P = 0.92) (**Fig. 1F**). Differential expression of these genes is thus likely regulated by factors other than chromatin exposure, such as transcription factor availability, histone modifications or DNA methylation.

Collectively, the above data indicate that the TFH-to-TR1 cell conversion involves extensive remodeling of the chromatin and massive silencing of TFH gene expression.

Contraction of the chromatin in pMHCII-NP-induced Tet+ vs. TFH cells at the bulk level

Bulk ATACseq studies of pMHCII-NP-induced Tet+ cells (~70% of which are TR1-like/TR1 cells; n=4) and KLH-induced TFH cells (~70% of which are TFH.1/TFH.2 cells; n=3) were consistent with the scMultiome data. KLH-induced TFH cells contained 13 times more differential OCRs (as compared to Tconv cells; n=3) than their BDC2.5mi/I-A^{g7}-NP-induced Tet+ counterparts (n=10,919 vs 821, respectively). Furthermore, the overwhelming majority of the chromatin regions that are differentially exposed in pMHCII-NP-induced Tet+ cells (as compared to Tconv controls) (97.9%) are also differentially exposed in KLH-induced TFH cells (**Fig. 2A and Datasheet 1**). This includes genes such as *Batf, Bhlhe40, Cxcr5, Icos, Il10, Il21, Lag3, Maf, Nt5e, Pdcd1, Stat3, Tcf7,* and *Tox2*. In addition, the chromatin regions that are differentially open in the pMHCII-NP-induced Tet+ and/or KLH-induced TFH cell pools (as compared to Tconv cells, where these OCRs are closed) are significantly associated with gene upregulation ($P < 7.88e-11$); no such association is found for genes linked to closed chromatin in either pMHCII-NP-induced Tet+ or KLH-induced TFH cells ($P = 0.86$) (**Fig. 2B and Datasheet 2**). Moreover, chromatin closure in BDC2.5mi/I-A^{g7}-NP-induced Tet+ cells relative to KLH-induced TFH cells was associated with downregulation of gene expression: 158 of the 341 genes that were downregulated in the former were linked to differentially closed OCRs (46.3%), as opposed to 94 of the 367 genes that were upregulated (25.6%) ($P = 1.38e-08$) (**Fig. 2C**).

Thus, studies of pMHCII-NP-induced Tet+ and KLH-induced TFH cells at the bulk level faithfully replicate the observations made using single cell Multiome. Together, they indicate that the TR1-like/TR1 cells contained within the Tet+ pool close a significant fraction of the chromatin as they transdifferentiate from TFH cells, leading to downregulation of gene expression, but the chromatin that remains open in TR1 cells is already exposed at the TFH cell stage. We acknowledge that, in the bulk ATAC-seq studies, the differences in the number of OCRs found in tetramer+ cells or KLH-induced TFH cells vs. naïve T cells may be influenced by the intrinsic oligoclonality of the tetramer+ T cell pool arising in response to repeated pMHCII-NP challenge

(6). However, we note that scATAC-seq studies of the tetramer+ T cell pool found similar differences between the oligoclonal tetramer+ TFH subpool and its (also oligoclonal) tetramer+ TR1 counterparts (i.e., substantially higher number of OCRs in the former vs. the latter relative to naïve T cells).

H3K4me3, H3K27me3 and H3K27ac marks in genes upregulated during the TFH-to-TR1 cell conversion are already in place at the TFH cell stage

Histones can positively and negatively regulate gene expression upon undergoing post-translational modifications on N-terminal residues via acetylation, methylation and ubiquitination of lysines; methylation and citrullination of arginines; or phosphorylation of serine, threonine or tyrosine (32). Although some of these histone modifications are not involved in gene regulation but rather occur upon gene activation and RNA polymerase elongation, they are considered good epigenetic indicators of the status of the chromatin.

H3 is the histone that undergoes more epigenetic modifications. Acetylation of this histone, at K9, K14, K18, K23 or K27 is consistently associated with active transcription, by neutralizing the positive charge of lysine residues, weakening the H3–DNA interaction and enhancing accessibility of the chromatin to the transcription machinery. Generally, deposition of acetylated H3K27 (H3K27ac) is associated with gene expression and allows the identification of active/inactive or poised enhancers and active promoters (33). Unlike histone acetylation, histone methylation is electrically neutral and can be both activating or repressing, depending on the extent and lysine residue(s) involved. H3K4me3 deposition at transcriptional start sites (TSS) is, like H3K27ac deposition, a marker of actively transcribed genes and is thought to imprint transcriptional 'memory' between generations (29). H3K27me3, generally found near CpG-rich promoters and intergenic regions, represses gene expression, even in the presence of H3K4me3, which prevents permanent silencing of the gene. The simultaneous presence of activating and repressing (bivalent) marks at the same location allows dynamic responsiveness to signals (34).

Deposition of H3K27me3, like H3K4me3, has been linked to genomic imprinting through cell generations (30).

The scMultiome dataset described above indicated that there were 545 genes that were associated with regions of the chromatin that remain exposed as TFH.1 cells differentiate into TR1-like/TR1 cells and/or, to a much lesser extent, appear *de novo* in the latter. We therefore focused on this list of genes to investigate whether their lack of expression at the TFH cell stage was associated with absence of active/poised enhancers and promoters or with presence of repressive histone marks.

H3K4me3

The KLH-induced TFH, pMHCII-NP-induced Tet+ and the Tconv subsets had a similar number of H3K4me3 marked regions/peaks (as defined via ChIPseq) (**Datasheet 3**). As expected, most of these H3K4me3 marks (78%) were found at TSSs (**Suppl. Fig. 2A, top) (Datasheet 3**). Representative chromosome track views are shown further below, on **Fig. 6**.

The heatmaps shown in **Figure 3A (left)** show that the overall H3K4me3 deposition landscape in BDC2.5mi/I-A^{g7}-NP-induced Tet+ cells (containing ~70% TR1 cells) is closer to that seen in KLH-induced TFH cells than in their Tconv counterparts (at the global level, including all chromatin regions, both open and closed at the TR1 cell stage) (**Datasheet 3**). **Fig. 3B (left)** shows the total number and relative percentage of differentially H3K4me3-marked regions (enriched for or depleted of H3K4me3) between KLH-induced TFH vs Tconv, BDC2.5mi/I-A^{g7}-NP-induced Tet+ vs. Tconv and BDC2.5mi/I-A^{g7}-NP-induced Tet+ vs. KLH-induced TFH cells, respectively (**Datasheet 4**). There were only 123 differentially marked H3K4me3 peaks between Tet+ and TFH cells (adjusted $P < 0.01$) and, in the scMultiome dataset, most of these were linked to areas of the chromatin that were closed in TR1 cells as compared to their TFH precursors, except for two genes (*Ptpn11* and *Angptl2*), suggesting that differential H3K4me3 deposition at these genes is due to differential chromatin exposure. Further analysis of the data revealed that

most of the H3K4me3 peaks found in genes linked to OCRs shared by TFH and TR1 cells at the single cell level (77.6%; P < 2.2e-16) were found in all three subsets (BDC2.5mi/I-A^{g7}-NP-induced Tet+, KLH-induced TFH cells, and Tconv cells), indicating that the corresponding genes are already marked for expression at both the naïve and TFH cell stages (**Datasheet 5**).

Thus, the genes associated with regions of the chromatin that remain open in TR1 cells have nearly identical H3K4me3 deposition landscapes in both Tet+ and TFH cells.

H3K27me3

We identified a total of 56,454 H3K27me3-marked peaks in the three subsets described above (**Datasheet 3**). KLH-induced TFH cells had a significantly higher number of H3K27me3-marked peaks than Tconv or BDC2.5mi/I-A^{g7}-NP-induced Tet+ cells (42,274 vs. 10,944 and 3,236, respectively) (P < 2.2e-16). These H3K27me3 marks were found at the TSS (27.13%), or at intronic (19.29%) or intergenic regions (30%) (**Suppl. Fig. 2A, middle) (Datasheet 3**).

The heatmaps shown in **Fig. 3A (middle; Datasheet 3)** show that, as was the case for H3K4me3, the overall H3K27me3 deposition landscape in pMHCII-NP-induced Tet+ cells is closer to that seen in TFH cells than in their Tconv counterparts. **Figure 3B (middle; Datasheet 4)** shows the number of differentially marked regions (enriched for or depleted of H3K27me3) between KLH-induced TFH vs Tconv, BDC2.5mi/I-A^{g7}-NP-induced Tet+ vs. Tconv and BDC2.5mi/I-A^{g7}-NP-induced Tet+ vs. KLH-induced TFH cells. There were only 167 differentially marked regions between Tet+ and TFH cells (adjusted P < 0.01), and most of these mapped to areas of the chromatin that are closed during the TFH.1 to TR1 transition, except for two genes (*Filip1l* and *Cdk8*). As was also the case for H3K4me3, most of the H3K27me3 marks found in genes associated with OCRs shared by both TFH and/or TR1 cells at the single cell level (95.8%; P < 2.2e-16) were shared by all three subsets (BDC2.5mi/I-A^{g7}-NP-induced Tet+, KLH-induced TFH cells, and Tconv cells), indicating that the corresponding genes already had this mark at the naïve and TFH cell stages (**Datasheet 5**).

H3K27Ac

As with H3K4me3, but unlike H3K27me3, the absolute number of H3K27Ac marks in each cell type were similar (~44,000/cell type). As expected, H3K27Ac marks were found at TSS (34%), intronic (24%) and intergenic locations (18%) (**Suppl. Fig. 2A, bottom)** (**Datasheet 3**).

The heatmaps shown in **Fig. 3A (right; Datasheet 3)** show that, as was the case for H3K4me3 and H3K27me3, the overall H3K27ac deposition landscape in BDC2.5mi/I-A^{g7}-NP-induced Tet+ cells is closer to that seen in KLH-induced TFH cells than in their Tconv counterparts. **Figure 3B (right; Datasheet 4)** shows the number of differentially marked regions (enriched for or depleted of H3K27ac) between KLH-induced TFH vs Tconv, BDC2.5mi/I-A^{g7}-NP-induced Tet+ vs. Tconv and BDC2.5mi/I-A^{g7}-NP-induced Tet+ vs. KLH-induced TFH cells. Remarkably, there were only 7 regions that were differentially marked with H3K27Ac between Tet+ and TFH cells (adjusted $P < 0.01$), in this case linked to *Cd247, Foxp1, Smco4,* and *Rab3ip*. Unlike the case for H3K4me3 and H3K27me3, most of the H3K27ac marks found in genes associated with OCRs shared by both TFH.1 and/or TR1 cells at the single cell level (73.8%; $P < 2.2e-16$), were shared by both BDC2.5mi/I-A^{g7}-NP-induced Tet+ and KLH-induced TFH but not Tconv cells (**Datasheet 5**), indicating that these genes were marked with H3K27ac at the TFH cell stage.

We note that, although in the representative chromosome track views shown in **Fig. 6C** there appear to be differences in the intensity of the peaks, thorough statistical analyses involving signal background for each condition and p-value adjustment did not support differential enrichment for histone deposition around the *Il10* gene between pMHCII-NP-induced tetramer+ T cells and KLH-induced TFH cells.

Collectively, these results suggest that most of the genes that are upregulated during the TFH-to-TR1 cell conversion have H3K4me3, H3K27me3 and H3K27ac marks that are already in place at the TFH stage.

The methylation status of most of the genes that remain accessible at the TR1 cell stage is already imprinted at the TFH stage

DNA methylation (DNAme) is based on the covalent binding of a methyl group to the C-5 position of a cytosine ring of DNA. In adult mammalian cells, 98% of DNA methylation targets cytosines in CpG dinucleotides, is directly associated with transcriptional silencing, and is maintained through cell division (i.e. is a heritable epigenetic trait) (35). Demethylation is an ultimate defining step of cell identity and is associated with long-term enhancer accessibility (36). Consequently, differentiated cells possess a stable and unique methylome structure that regulates their cell-specific transcriptomic profile.

To investigate the potential contribution of changes in DNA methylation to gene expression as BDC2.5mi/I-A^{g7}-NP-induced TFH.1 cells transdifferentiate into TR1 cells, we performed genome-wide bisulfite sequencing of BDC2.5mi/I-A^{g7}-NP-induced Tet+, KLH-induced TFH cells and Tconv cells. We focused our analysis on differentially methylated regions (DMRs; q value < 0.05) (**Datasheet 6**). Among all the DMRs found in BDC2.5mi/I-A^{g7}-NP-induced Tet+ and KLH-induced TFH cells vs. Tconv cells, 43.2% were shared by BDC2.5mi/I-A^{g7}-NP-induced Tet+ and KLH-induced TFH cells, 33.9% were unique to KLH-induced TFH cells and 24.8% were unique to BDC2.5mi/I-A^{g7}-NP-induced Tet+ cells (**Fig. 4A and Datasheet 6**).

Most of these DMRs were primarily found in intronic CpG islands, followed by exonic and then intergenic regions and gene promoters (**Suppl. Fig. 3 and Datasheet 6**). The differentially hypomethylated regions found in BDC2.5mi/I-A^{g7}-NP-induced Tet+ cells relative to Tconv cells were associated with 2,714 genes. Most of these genes (70%; P < 2.2e-16) were also differentially hypomethylated in KLH-induced TFH cells (**Fig. 4B, left; Datasheets 6 and 7**). Likewise, of the 2,748 genes that were associated with differentially hypermethylated regions in BDC2.5mi/I-A^{g7}-NP-induced Tet+ cells, most (71%; P < 2.2e-16) also harbored differentially hypermethylated regions in KLH-induced TFH cells (**Fig. 4B, right; Datasheets 6 and 7**). **Figure 4C** provides a

graphical representation of the genic location of these DMRs as a function of whether they are shared between Tet+ and TFH vs. Tconv cells and their methylation status. Thus, BDC2.5mi/I-A^{g7}-NP-induced Tet+ cells and KLH-induced TFH cells share a remarkably similar methylome (**Datasheet 6**).

We next focused our attention on genes whose chromatin was accessible in both TFH.1 and TR1 cells as determined by scATACseq (i.e., excluding genes silenced by chromatin closure). We classified these genes into three groups: 1) carrying DMRs in BDC2.5mi/I-A^{g7}-NP-induced Tet+ but not KLH-induced TFH cells; 2) carrying DMRs in KLH-induced TFH cells but not BDC2.5mi/I-A^{g7}-NP-induced Tet+ cells; and 3) shared by both populations. Notably, 328 of 545 genes associated with accessible chromatin in both TFH and TR1-like/TR1 cells at the single cell level harbor DMRs in BDC2.5mi/I-A^{g7}-NP-induced Tet+ and/or KLH-induced TFH cells vs. Tconv cells, and most of these genes (87.5%; $P < 1.85e-5$) have a similar methylation status in both BDC2.5mi/I-A^{g7}-NP-induced Tet+ and KLH-induced TFH cells (n=236 hypomethylated; n=51 hypermethylated) (**Fig. 4D and Datasheet 8**). Thus, the genes that remain accessible during the TFH-to-TR1 cell differentiation process, share an even greater degree of DNA methylation status than when considering all genes regardless of chromatin accessibility.

Of the 328 accessible genes associated with DMRs in BDC2.5mi/I-A^{g7}-NP-induced Tet+ and/or KLH-induced TFH cells vs. Tconv cells, 159 (48.5%) were differentially expressed between TR1 and TFH cells as determined by scRNAseq. As expected, based on the data shown above, there was no correlation between methylation status and differential gene expression (**Fig. 4E and Datasheet 8**) (P=0.92). Although most of the accessible genes sharing their methylation status in both BDC2.5mi/I-A^{g7}-NP-induced Tet+ and KLH-induced TFH cells were not differentially expressed in TR1 vs. TFH.1 cells (50.2%), 41.1% were downregulated (e.g., *Cxcr5, Il21, Pdcd1, Ctla4, Tigit*, *Maf, Nfia and Tox2*) and 8.7% were upregulated (e.g., *Il10, Bach2 and Tbx21*).

This apparent inheritance of gene methylation status by pMHCII-induced TR1 cells from their TFH precursors is further illustrated by direct comparison of the methylation status of TFH

and TR1-specific genes, such as *Il2* and *Il10*, or genes expressed by both, such as *Il21*. *Il2* is highly expressed in TFH but not TR1 cells and yet it is differentially hypomethylated in both BDC2.5mi/I-A^{g7}-NP-induced Tet+ and KLH-induced TFH cells as compared to Tconv cells (**Suppl. Fig. 4, left**). Likewise, *Il10*, which is expressed by TR1 cells but not TFH cells is already significantly hypomethylated in several regions upstream of the TSS in KLH-induced TFH cells (and BDC2.5mi/I-A^{g7}-NP-induced Tet+ cells) as compared to their Tconv counterparts; in fact, when these two cell subsets are compared directly to each other, only relatively minor differences in the methylation status of *Il2* and *Il10* can be seen (**Suppl. Fig. 4, middle**). As expected, *Il21*, expressed by both TFH and TR1 cells, is also hypomethylated in both T cell subsets as compared to Tconv cells (**Suppl. Fig. 4, right**).

Collectively, the above data suggest that the methylation status of most of the genes that remain accessible at the TR1 cell stage is already imprinted at the TFH stage, and that most gene expression differences between TR1 and TFH cells cannot be accounted for changes in the overall methylation status of the corresponding genes. In a small number of cases, however, the TFH-to-TR1 cell conversion is accompanied by further gene demethylation of TR1-specific genes (i.e. *Il10*) and remethylation of TFH-specific ones (i.e., *Cxcr5*).

Changes in gene expression during the TFH to TR1 cell conversion are largely dissociated from re-distribution of epigenetic marks. To further define the contribution of the various epigenetic modifications discussed above on gene expression, we again focused on the genes associated with chromatin regions that remain open as TFH cells become TR1. We then ranked these genes according to gene expression changes, from upregulated to downregulated in TFH or Tet+ cells as compared to Tconv cells (**Suppl. Figs. 5-6**) or in Tet+ vs. TFH cells (**Suppl. Fig. 7**) (**Datasheet 9**). Whereas for most genes, differential gene expression in TFH or Tet+ vs Tconv cells is associated with differential gene methylation, open chromatin, and H3K27ac and/or

H3K4me3 deposition, very few differences were noted in all these readouts when comparing Tet+ to TFH cells.

Loss of TFH-specific transcription factor gene expression during the TFH-to-TR1 conversion is associated with chromatin closure

The above data collectively suggest that transdifferentiation of TFH cells into TR1 cells is driven by changes in the expression of TFH-stabilizing and TR1-promoting transcription factors (TFs). This, coupled to the extensive closure of chromatin sites in TFH cells as they become TR1 cells, suggested that changes in TF expression, particularly the loss of TFH-associated TFs, might be driven, in part, via chromatin remodeling of the coding loci. To investigate this, we compared the types and direction (expression-promoting or suppressing) of the various epigenetic modifications studied above on TF-coding genes as a function of upregulation or downregulation. As shown on **Fig. 5 (Datasheet 10)**, the TF-coding genes that are downregulated during the TFH-to-TR1 conversion, unlike those that are upregulated (based on the scMultiome data), close a significant number of OCRs (13/29 of downregulated TF-coding genes had closed OCRs, as compared to only 4/38 of upregulated TF-coding genes, ($P<0.0001$). As expected, based on the epigenetic similarity of TFH vs. TR1 cells, upregulation of TF-coding genes was largely dissociated from the epigenetic marks studied here.

TR1 cells inherit active enhancers from their TFH precursors

Gene expression is driven by the sequential recruitment of DNA-binding transcription factors (TFs; bound to proximal promoters and/or distal GREs), non-DNA-binding cofactors and the transcription machinery to the core promoter. Enhancers are GREs that positively activate transcription in primed gene promoters found thousands of kb away and even on different chromosomes but are proximal in the three-dimensional structure of the chromatin in the nucleus.

Whereas active enhancers are typically marked with H3K4me1, H3K27ac and some H3K4me3, poised enhancers contain both H3K4me1 and the repressive H3K27me3 mark (33, 37-39). Active enhancers target genes marked with H3K27ac and H3K4me1 at and downstream of their TSS, respectively (33, 37-39).

Thus, whereas ATACseq helps to identify areas of open chromatin associated with various regulatory elements such as enhancers, silencers, and promoters, H3K27Ac ChIPseq helps locate class I active enhancer and promoter elements. To map the location of active enhancers in BDC2.5mi/I-A^{g7}-NP-induced Tet+ cells and KLH-induced TFH cells, we carried out an integrated analysis of both datasets (areas of open chromatin and H3K27ac deposition) in both cell pools. OCRs containing H3K27Ac peaks, excluding those located within 2 kb of the TSS (i.e., overlapping promoters), were considered to represent active enhancers. As expected, based on the data presented above, the BDC2.5mi/I-A^{g7}-NP-induced Tet+ pool shared significantly more active enhancers with KLH-induced TFH cells (n=6,767/8,444; 80.2%) than with Tconv cells (n=4,685/8,444; 55.5%) ($P < 2.2e-16$) (**Fig. 6A and Datasheet 11**).

We next focused on active enhancers proximal to genes linked to accessible chromatin in both TFH and TR1 cells, as defined via scATACseq. We divided the corresponding active enhancers into three sub-groups: 1) those exclusively found in BDC2.5mi/I-A^{g7}-NP-induced Tet+ cells; 2) only found in KLH-induced TFH cells, and 3) shared by both cell types. As shown in **Fig. 6B**, most of the genes that remain open as the cells transition from the TFH state to its TR1 counterparts (i.e. are not closed), already harbor active enhancers in TFH cells. Specifically, most of the 396 genes that are associated with accessible chromatin in both TR1-like/TR1 and TFH cells and are marked with active enhancers (89.6%; $P < 2.2e-16$), display such enhancers in both the BDC2.5mi/I-A^{g7}-NP-induced Tet+ and KLH-induced TFH pools.

We then investigated whether differences in the expression of these genes, as defined via scRNAseq, were associated with differences in the number and/or location of active enhancers. As expected, given the high epigenetic poised state for genes upregulated at the TR1 cell stage,

at the precursor (TFH) cell stage for all readouts examined so far, there was no significant correlation between active enhancer distribution and differential gene expression (**Fig. 6B and Datasheet 12**) (P=0.76). In fact, as also noted for genes associated with chromatin regions that remained open at the TR1 cell stage, which were mostly downregulated (**Fig. 1F**), most genes marked with active enhancers at the TFH stage (68.9%; P < 2.2e-16) were downregulated in TR1 cells (e.g., *Cxcr5, Il21, Pdcd1, Tigit, Egr2, Maf, Nfia and Tox2* to name a few).

Together, these data suggest that: (1) most of the genes that remain open as BDC2.5mi/I-A^{g7}-NP-induced TFH cells transition into TR1-like/TR1 cells also share active enhancers in both subsets; and (2) differences in the expression of these genes are likely mediated by other factors, such as DNA demethylation and/or differential TF availability.

Most of the upregulated genes at the TR1 stage had already demethylated their distal GREs at the TFH stage

Detailed analyses of the intergenic DMRs found in KLH-induced TFH cells (and shared with BDC2.5mi/I-A^{g7}-NP-induced Tet+ cells) revealed a striking overlap with active enhancers. **Fig. 6C** illustrates the location of DMRs around *Il10* locus relative to the various transcriptional and epigenetic readouts explored herein, including active enhancers, in Tconv, BDC2.5mi/I-A^{g7}-NP-induced Tet+ and KLH-induced TFH cells. Several lines of evidence suggest that the patterned hypomethylation status of distal gene regulatory elements of TR1 genes in TFH precursors define the TR1-poised nature of the TFH epigenome. First, DNA methylation is generally not permissive for transcription (35), even at active enhancers. Second, enhancer de-methylation is highly cell type-specific and accurately predicts target gene transcription (40). Third, differential methylation among cell types is greatest at distal gene regulatory elements than in promoters (40, 41). Finally, de-methylation at these sites appears to be a required final step in enhancer activation during cell fate transitions, leading to the stabilization of cell line identity (36).

To reveal the identity of differentially expressed genes proximal to 'distal' gene regulatory regions (GREs) marked by open chromatin, H3K27ac deposition and hypomethylation (excluding promoters), we interrogated our active enhancer dataset for Tet+ and TFH-specific differentially methylated regions (vs. Tconv cells). The vast majority of DMRs mapping to active enhancers found in BDC2.5mi/I-A^{g7}-NP-induced Tet+ cells (92.5%; P < 2.2e-16) were hypomethylated (including *Icos, Ctla4, Pdcd1, Tigit, Il10, Irf4, Maf* and *Prdm1)* (**bottom pie chart in Fig. 7A** (**Datasheet 13**). This was also true for KLH-induced TFH cells (n=1051/1,185; 88.7%; P < 2.2e-16) (e.g., *Cxcr5, Il10, Il21, Bach2, Nfil3, Nfil3* and *Tox2*) (**middle pie chart in Fig. 7A** (**Datasheet 13**). In fact, a large fraction of the differentially methylated active enhancers found in these subsets were shared between BDC2.5mi/I-A^{g7}-NP-induced Tet+ and KLH-induced TFH cells (65% and 35%, respectively (**Euler's plot in Fig. 7A**) (**Datasheet 13**). In contrast, only 10% and 10.71% of differentially methylated active enhancers found in BDC2.5mi/I-A^{g7}-NP-induced Tet+ cells and KLH-induced TFH cells, respectively, were shared with Tconv cells (**Euler's plot in Fig. 7A**) (P = 0.02) (**Datasheet 13**). In addition, most of the DMRs overlapping active enhancers found in TFH and Tet+ cells (92.1%) are hypomethylated (**top pie chart in Fig. 7A**) (**Datasheet 13**).

We next explored the methylation status of active enhancers linked to genes that remain accessible as TFH cells transdifferentiate into TR1 cells. The differentially methylated enhancers linked to these genes were classified as: 1) specific for BDC2.5mi/I-A^{g7}-NP-induced Tet+ cells; 2) specific for KLH-induced TFH cells; and 3) shared by both BDC2.5mi/I-A^{g7}-NP-induced Tet+ and KLH-induced TFH cells as compared to Tconv cells. Notably, most of these differentially methylated enhancers (66%) were shared by Tet+ and TFH cells. As with most other readouts examined herein, there was no statistically significant association between the presence of differentially hypo- or hypermethylated active enhancers and overall gene expression differences (**Fig. 7B**; P=1) (**Datasheet 13**). This observation is consistent with the idea that the methylation status of distal GREs for genes specifically upregulated in TR1 cells is almost invariably imprinted at the TFH stage, thus indicating that TFHs are epigenetically poised to acquire a TR1

transcriptional profile. The *Il10* locus, for example, whose expression is significantly upregulated in BDC2.5mi/I-A^{g7}-NP-induced Tet+ cells as compared to KLH-induced TFH cells, harbors 8 and 6 differentially hypomethylated active enhancers in Tet+ and TFH samples, respectively, as compared to Tconv cells (**Fig. 6C**). Thus, most of the upregulated genes at the TR1 stage appear to have already de-methylated their distal GREs at the TFH stage.

Active enhancers at genes specifically upregulated at the TR1 cell stage are enriched for binding sites for the TFH/TR1 transcription factors TOX-2, IRF4, and c-MAF

We next sought to investigate if the putative active enhancers identified in BDC2.5mi/I-A^{g7}-NP-induced Tet+ and KLH-induced TFH cells contained binding sites for the TFH transcription factors TOX-2, IRF4, and c-MAF. The genes that were upregulated at the TR1 cell stage and shared an open chromatin status with TFH cells, based on the scMultiome dataset, were associated with 285 active enhancers. We then mapped ChIPseq peaks for TOX-2 from TFH cells, and IRF4 and c-MAF from Th17 cells (42-44) onto these active enhancers. Remarkably, 34.4%, 66.3% and 70.1% of these enhancers had TOX-2, IRF4, and c-MAF binding sites, respectively, and ~61% of these TF-binding active enhancers are already present in TFH cells (vs. <2% in Tconv cells; P < 3.03e-8) (**Fig. 7C and Datasheet 14**).

Thus, many of the active enhancers linked to genes specifically upregulated at the TR1 cell stage, which, in turn, are highly hypomethylated and accessible at the TFH cell stage, are enriched for binding sites for all the three TFH TFs studied herein: TOX-2, IRF4, and c-MAF. Therefore, these sites are likely already occupied by these TFs at the TFH stage, especially considering their described role in TFH development and maintenance. For example, many hypomethylated active enhancers linked to *Il10 in* BDC2.5mi/I-A^{g7}-NP-induced Tet+ cells and KLH-induced TFH cells have binding sites for TOX-2 (as well as IRF4 and c-MAF) in TFH and Th17 cells (**Fig. 6C**).

Discussion

Having established that TFH cells can transdifferentiate into TR1-like and terminally differentiated TR1 cells *in vivo* in response to certain stimuli (6, 7), we sought to explore the epigenetic events underpinning this process. Our comprehensive transcriptional and epigenetic studies at the bulk and/or single cell levels indicate that conventional antigen experienced TFH cells are epigenetically poised to become TR1 cells. One of our main findings is that the TFH-to-TR1 differentiation process is associated with massive closure of OCRs, and that the vast majority of the OCRs found in TR1-like and TR1 cells are also found in KLH-DNP-induced TFH cells. Furthermore, most of the genes harbored in these shared OCRs, such as *Cxcr5, Tox2, Il21, Il10,* and *Ctla4*, to just name a few, contain nearly identical patterns of histone deposition marks, including H3K4me3, H3K27me3 and H3K27Ac, equally similar DNA methylation patterns in gene bodies, proximal promoters and gene-distal regulatory elements and a similar distribution of active enhancers across the genome, even when not expressed in either cell type. Altogether, these data indicate that the TR1-poised epigenome of TFH cells is a key enabler of this transdifferentiation process, and that transdifferentiation of TFH cells into TR1 cells is likely driven by changes in the expression of TFH-stabilizing and TR1-promoting transcription factors, possibly in response to sustained ligation of TCRs.

Our earlier scRNAseq and mass cytometry studies of cognate (antigen-specific, tetramer+) pMHCII-NP-induced CD4+ T cells demonstrated the presence of a significant Tet^{+} TFH-like cluster that separated away from its TR1 counterpart (6, 7). When compared to each other, these two major clusters of tetramer^{+} cells were remarkably similar, but the TR1 sub-pool had significantly downregulated key TFH-specific genes, including *S1pr2*, *Cxcr4*, *Cxcr5*, *Pdcd1*, *Il4*, *Ascl2*, *Bcl6*, *Cba2t3*, *Cebpa*, *Id3*, *Nfia*, *Pou2af1*, *Tox2*, while upregulating TR1-associated genes, such as *Ccr5*, *Havcr2*, *Il10*, *Ahr*, *Myc* and *Prdm1*. Importantly, these two clusters were developmentally related because they harbored identical clonotypes (i.e. identical TCR$\alpha\beta$

sequences at different transcriptional states). Additional studies indicated that the TFH-to-TR1 conversion proceeds through a transitional TR1-like subset, whereby the progenitors undergo progressive downregulation of TFH-associated transcripts (i.e., *Bcl6, Cxcr5*, among others) and progressive upregulation of TR1-associated transcripts (i.e. *il10, Ccr5* and *Prdm1*, among others). The suspected TFH origin of pMHCII-NP-induced TR1 cells was further supported by two additional lines of evidence. First, treatment of NOD.*Scid* mice engrafted with total CXCR5^{high}PD-1^{high} CD4^{+} T-cells (containing pMHCII-NP-expanded TFH-like cells but devoid of terminally differentiated Tet+ TR1 cells) with pMHCII-NPs led to formation of cognate TR1-like and terminally differentiated TR1 cell pools in the hosts. Second, the two-dimensional scMultiome profile of Tet+ TFH-like cells arising in response to BDC2.5mi/IA^{g7}-NP therapy was essentially identical to that corresponding to an effector TFH-like sub-pool of TFH-like cells (CD4^{+}CD44^{hi}CXCR5^{hi}PD1^{hi}) induced by immunization with the KLH-DNP conjugate (*Bcl6^{hi}Tox2^{hi}Il21^{+}Pdcd1^{+}*; referred to as TFH.1).

Abrogation of *Prdm1* (encoding BLIMP-1) expression enabled the conversion of TFH.1 cells into TR1-like progeny, but completely blunted the TR1-like–>TR1 conversion, indicating that this process requires the expression of BLIMP-1, a transcriptional repressor that antagonizes BCL-6 expression and function in both B- and T-cells, including TFH cells (45). Since expression of BLIMP-1 in T-cells is restricted to activated T-cells and is induced by TCR ligation], and since pMHCII-NP therapy triggers the formation and expansion of cognate, antigen-specific TR1-like cell pools via sustained TCR signaling (2), we suspect that BLIMP-1 expression in TFH cells is induced by repetitive encounters of cognate TFH cells with these compounds. Progressive downregulation of *Bcl6* and upregulation of *Prdm1* at the TR1-like cell stage, immediately preceding TR1 development, might be facilitated by the loss of *Lef1* and significant downregulation of *Tcf7* (endocing TCF-1) expression (positive regulators of *Bcl6* expression and negative regulators of *Prdm1* expression) in pMHCII-NP-challenged vs. vaccine-induced TFH cells. In fact, the Tet^{+} TR1-like and terminally differentiated TR1 cells (BLIMP-1-independent or -

dependent, respectively) differ in the expression levels of a significant number of genes whose expression has been previously associated with this transcription factor, including *Il10, Ctla4, Lag3, Icos, Havcr2, Tnfrsf4* and *Tnfrsf18*, among others (46).

Here, we have shown that pMHCII-NP-driven transdifferentiation of cognate TFH cells into TR1 progeny is driven by both massive closure of OCRs and major changes in the transcriptional factor make-up of the cells, rather than by TCR signaling-induced changes in the epigenetic status of the genes contained within the shared OCRs. There are some noteworthy differences between the evolution of the epigenetic landscape in effector, memory and exhausted T cells as compared to what we see in the TFH-TR1 pathway. In T cells, acquisition of the epigenetic programs of effector, memory and exhaustion states are stepwise processes. In exhausted T cells, for example, ATACseq and H3K27AC ChIPseq analyses of different exhausted states are associated with distinct epigenetic states, including differential chromatin accessibility and active enhancer landscapes, yet shared transcription factor profiles (11). In contrast, transdifferentiation of TFH cells into TR1 cells appears to be driven by changes in the expression of TFH-stabilizing and TR1-promoting transcription factors, in the face of remarkable epigenetic similarity, including a shared methylome, consistent with the idea that TFH cells are poised to rapidly become TR1 when appropriately activated. Interestingly, the TF-coding genes that are significantly downregulated during the TFH-to-TR1 conversion, unlike those that are upregulated, experience a significant reduction in chromatin accessibility. In contrast, as expected based on the epigenetic similarity of TFH vs. TR1 cells, upregulation of TF-coding genes important for TR1 cell genesis is largely dissociated from the different epigenetic marks studied here, including changes in chromatin accessibility. This suggests that changes in TF expression, particularly the loss of TFH-associated TFs, are driven, in part, via chromatin remodeling of the coding loci.

The combination of transcription factors that become available (i.e. *Prdm1*) or unavailable (i.e. *Bcl6*) during the TFH-TR1 conversion would be responsible for enabling/driving the formation of the active enhancer-promoter contacts required for gene expression and establishing TR1

transcriptional identity. This would explain why TR1-associated genes that are already epigenetically marked for expression in TFH cells (i.e. *Il10*) remain silent at the TFH stage. This is not a unique feature of the TFH-to-TR1 transdifferentiation process. For example, although the *Il10* locus is closed and transcriptionally silent in naive CD4+ T cells, it is exposed (47) and incorporates permissive H3K4me3 marks but not repressive H3K27me3 marks in differentiated T helper subsets (42, 48), promoting a transcriptional competent yet silent state. Since transcription factors regulating Th1, Th2 and Th17 subsets, including T-bet, GATA-3 or RORγt, do no inhibit IL-10 expression, but rather enhance it, the above observations imply that different effector cell programs can co-exist with much broader gene expression-competent states. Our data indicate that this is also true for TFH cells. In fact, the expression of *Il10* in Th cell subsets can only occur until the transcription factors required for gene expression become available. For example, BATF (an AP1 family member), IRF4, NFAT, c-MAF, AHR and BLIMP-1 are known to collectively promote *Il10* expression by binding to the promoter and/or cis-regulatory elements of *Il10* (49). Likewise, although Th lineage-specific cytokines present active histone marks in the corresponding lineage and repressive marks in the others, transcription factor-coding genes are not always so strictly marked and display expression-permissive epigenetic patterns. For example, *Tbx21*, encoding T-bet, harbours activating H3K4me3 marks in the promoter of Th1 cells, but bivalent modifications in other Th subsets. This is also true for *Gata3* and *Rorc* or *Bcl6* in Th2 vs non-Th2, Th17 vs. non-Th17 and TFH vs. non-TFH cells, respectively (50, 51). Thus, whereas *Bcl6* is also marked with expression-promoting H3K4me3 marks in other Th cell subsets, loci encoding Th subset-specifying transcription factors (*Tbx21*, G*ata3* and *Rorc*) also appear to be poised for expression in TFH cells (50). Because BCL-6 can regulate the expression other transcription factors, it is likely the collective transcription factor make-up of the cell that determines its phenotype at a given point in time. It is thus reasonable to suspect that the epigenomes of polarized T cell subsets, including TFH cells, are programmed to enable their

conversion into alternative transcriptional states when required (i.e, in response to excessive antigenic stimulation).

The TR1-poised state of TFH cells is also reflected on the global active enhancer landscapes of both cell types. For example, we have shown that most of the genes that remain open as BDC2.5mi/I-A^{g7}-NP-induced TFH.1 cells transition into TR1-like/TR1 cells also share active enhancers in both subsets. In addition, the de-methylated status of most active enhancers associated with genes specifically upregulated in TR1 cells, such as *Il10*, were already so (hence imprinted) at the TFH stage. Furthermore, we find that many of the active enhancers linked to genes specifically upregulated at the TR1 cell stage, which, in turn, are highly hypomethylated and accessible at the TFH cell stage, are enriched for binding sites for at least three TFH-associated TFs, including TOX2, IRF4, and c-MAF. This suggests that these sites are likely already occupied by these TFs at the TFH stage. The remarkable similarity of the DNA methylome of the TFH and TR1 subsets further suggests that both TFH and TR1 cells share a stable epigenetic program.

The factors responsible for chromatin closure during the TFH-to-TR1 conversion remain to be determined, but changes in the expression of *Tox2* (and the related transcription factor *Tox*) may contribute to this event. TOX-2 expression in CD4+ T-cells is upregulated by BCL-6, and TOX-2 binds to loci associated with TFH generation, including *Bcl6*, *Cxcr5*, *Pdcd1* (also upregulated in TR1-like cells) along with BATF and IRF4 or STAT-3, increasing their chromatin accessibility and promoting their expression (44). Importantly, whereas KLH-DNP- and pMHCII-NP-induced TFH cells express high levels of *Tox2*, their TR1-like and TR1 counterparts express substantially lower levels; suboptimal occupation of TOX-2 binding sites by TOX-2 in pMHCII-NP-challenged TFH cells may result in the closure of these sites, cessation of the expression of the corresponding genes and progressive differentiation into TR1 cells. Downregulation of TCF-1 (encoded by *Tcf7*) and LEF-1 expression as TFH cells become TR1 cells may be additional contributing factors to loss of chromatin accessibility (52). We note that loss of TCF-1 in T cell

subsets is usually paralleled by loss of LEF-1, which belongs to the same TF family and recognizes a similar motif (52). In developing thymocytes, upregulation of TCF-1 expression is associated with an increase in chromatin accessibility, suggesting that it may act as a pioneer TF. Furthermore, loss of TCF-1 in DP thymocytes or CD8+ T cells, T-exhausted stem cells or activated CD4+ or CD8+ T cells is associated with loss of chromatin accessibility at sites that had bound TCF-1 (52). In addition, TCF-1, along with CTCF, promotes deposition of H3K27ac onto insulated enhancers and the recruitment of cohesin-loading factor NIPBL at active enhancers in developing thymocytes (53). In another recent study, TCF-1 was identified as a “placeholder” TF, responsible for maintaining chromatin accessibility in naïve T cells, and allowing activation-induced TFs to displace it (54). Hence, downregulation of TCF-1 and LEF-1 may contribute to the loss of the TFH-specific gene expression program as these cells transdifferentiate into TR1, close previously open chromatin sites, and acquire new transcription factors orchestrating the TR1-specific gene expression program.

The current study provides a foundational understanding of how the epigenetic landscape of TFH cells evolves as they transdifferentiate into TR1 progeny in response to chronic ligation of cognate TCRs using pMHCII-NPs. Our current studies focus on functional validation of these observations, by carrying out extensive perturbation studies of the TFH-TR1 transdifferentiation pathway in conditional transcription factor gene knock-out mice. In these ongoing studies, genes coding for a series of transcription factors expressed along the TFH-TR1 pathway are selectively knocked out in T cells, to ascertain (i) the specific roles of key transcription factors in the various cell conversion events and transcriptional changes that take place along the TFH-TR1 cell axis; (ii) the roles that such transcription factors play in the chromatin re-modeling events that underpin the TFH-TR1 transdifferentiation process; and (iii) the effects of transcription factor gene deletion on phenotypic and functional readouts of TFH and regulatory T cell function. Although the TFH-TR1 transdifferentiation was discovered in mice treated with pMHCII-NPs, we now have evidence that this is a naturally occurring pathway that also develops in other contexts (i.e., in mice that

have not been treated with pMHCII-NPs). Importantly, the discovery of this transdifferentiation process affords a unique opportunity to further understand the transcriptional and epigenetic mechanisms underpinning T cell plasticity; the findings reported here can help guide/inform not only upcoming translational studies of pMHCII-NP therapy in humans, but also other research in this area.

Although the snapshot provided by our single cell studies reported herein documents the simultaneous presence of the different subsets composing the TFH-TR1 cell pathway upon the termination of treatment, the transdifferentiation process itself is extremely fast, such that proliferated TFH cells already transdifferentiate into TR1 cells after a single pMHCII-NP dose (6). This makes it extremely challenging to pursue dynamic experiments. Notwithstanding this caveat, ongoing studies of cognate T cells post treatment withdrawal, coupled to single cell studies of the TFH-TR1 pathway in transcription factor gene knockout mice exhibiting perturbed transdifferentiation processes are likely to shed light into the progression and stability of the epigenetic changes reported herein.

We have recently shown that αGalCer/CD1d-NPs can trigger the differentiation of liver-resident invariant NKT cells (LiNKT) into a TR1-like immunoregulatory, IL-10+IL-21-producing Zbtb16^{high}Maf^{high}Tbx21^{+}Gata3^{+}Rorc^{-} subset (LiNKTR1) that can suppress local inflammatory phenomena (55). Interestingly, epigenetic studies of liver iNKT cells both before and after *in vivo* delivery of aGalCer/CD1d-coated NPs have shown that unlike the case for pMHCII-NP-induced TR1 transdifferentiation, aGalCer/CD1d-NP-induced LiNKTR1 transdifferentiation involves the acquisition of a novel epigenetic state. Specifically, whereas for most genes, gene upregulation during the LinKT-to-LiNKTR1 cell transition is largely associated with treatment-induced hypomethylation, the most upregulated genes (i.e. *Il10* and *Il21*, among others) are also those that accumulate additional epigenetic modifications favoring gene expression, such as acquisition of new OCRs and H3K27ac and H3K4me3 marks. Thus, whereas TFH cells largely require chromatin closure and changes in transcription factor expression to become TR1 cells, LiNKT

cells do not undergo massive changes in chromatin exposure and involve extensive gene de-methylation to do so. Although the mechanisms underlying these differences remain unclear, they indicate that the processes that regulate responses of different T cell types to similar cues are context-dependent and dynamic.

Materials and Methods

Mice. NOD/ShiLtJ mice were from the Jackson Lab (Bar Harbor, ME, USA). The experiments described herein were approved by the Cumming School of Medicine's Animal Care Committee at the University of Calgary Animal Care and by the Animal Care Committee at Universitat de Barcelona.

pMHCII production. Recombinant pMHC class II were produced in CHO-S cells transduced with lentiviruses encoding peptide-MHC□ and MHC□ chains and IRES-CFP and IRES-EGFP cassettes, respectively, as described (56). Briefly, transduced CHO cells were grown in 2L baffled flasks (Nalgene, Thermo Fisher Scientific, Waltham, MA, USA) at 125 rpm, 5% CO_2 and 37ºC. Basal medium was Power-CHO-2 (Lonza, Basel, Switzerland) supplemented with 8 mM Glutamine (Cultek, Madrid, Spain) and Gentamicine Sulfate (0.25 mg/mL) (Lonza). The cultures were started in a volume of 400 mL of basal medium at a cell density of 350,000-400,000 cells/mL and were supplemented with Cell Boost 7a (Hyclone) at 3% v/v and Cell Boost 7b (Hyclone, GE Healthcare, Chicago, IL, USA) at 0.3% v/v on days 0, 3, 4, 5, 6, 8, 9 and 10. Temperature shift to 34ºC was done when cell densities reached 5-7x10^6 cells/mL. Additional Glutamine was added on day 7, to 2 mM. Glucose was added to 4.5 g/L when levels dropped below 3.5 g/L. Cells were harvested on Day 14 or when viability fell below 60%. The secreted proteins were purified by sequential affinity chromatography on nickel and strep-tactin columns and used for NP coating or biotinylated *in vitro* to produce pMHCII tetramers.

pMHCII tetramers. Phycoerythrin (PE)- or APC-conjugated tetramers were prepared using biotinylated pMHCII monomers and used to stain peripheral T-cells. Briefly, pMHCII monomers were subjected to biotinylation using Biotin ligase (Avidity, Aurora, CO, USA) following the supplier's protocols, and biotinylated monomers purified by ion exchange chromatography using

an AKTA FPLC system (GE Healthcare, Chicago, IL, USA). The final product was verified by denaturing SDS-PAGE. Tetramers were generated by adding PE-conjugated streptavidin (Life Technologies, Carlsbad, CA, USA) at a 4:1 molar ratio.

Flow cytometry for pMHCII-NP-induced Tet+ cells and KLH-DNP-induced TFH cells. To stain mononuclear cell suspensions from mice, splenic CD4+ T-cells were incubated with avidin for 15 min at room temperature and stained with tetramer (5μg/mL) in FACS buffer (0.05% sodium azide and 1% FBS in PBS) for 30 min at 4°C, washed, and incubated with FITC-conjugated anti-CD4 (RM4-5 or GK1.5 from BD Biosciences, San Diego, CA; 5μg/mL) and PerCP-conjugated anti-B220 (RA3-6B2 from BD Biosciences; 2μg/mL; as a 'dump' channel) for 30 minutes at 4°C, in the presence of an anti-CD16/CD32 mAb (2.4G2; BD Biosciences, or Biolegend, San Diego, CA, USA) to block Fc receptors. Cells were washed, fixed in 1% paraformaldehyde (PFA) in PBS and analyzed with FACSaria, or BD LSRII flow cytometers. Analysis was done using FlowJo software (FlowJo, BD Biosciences, San Diego, CA, USA).

TFH cells (PD-1^{hi}CXCR5^{hi}) were generated by immunizing NOD mice intraperitoneally with KLH (keyhole limpet hemocyanin) or KLH-DNP (Sigma-Aldrich, St. Louis, MO, USA) 3 times (100 μg/dose, CFA+IFA+IFA) once a week for three consecutive weeks. Splenic T-cells were stained with anti-CD4-Pacific Blue (GK1.5, BD Biosciences), anti-CD45R-PerCP (BD Biosciences), anti-CD44-FITC (IM7 from BD Biosciences), anti-CXCR5-biotin (2G8 from BD Biosciences), and anti-CD279-BV421 (PD-1; J43 from BD Biosciences) mAbs for 30 minutes at 4 ºC and with streptavidin-APC for 20 minutes at 4 ºC. TFH cells were identified within the CD4+CD45R– CD44^{hi} gate as cells expressing high levels of CXCR5 and CD279 (PD-1).

Nanoparticle synthesis. Maleimide-functionalized, pegylated iron oxide NPs (PFM series) were produced in a single-step thermal decomposition in the absence of surfactants as described recently (2). Briefly, 3g Maleimide-PEG (2 kDa MW, Jenkem Tech USA) were melted in a 50mL

round bottom flask at 100°C and then mixed with 7 mL of benzyl ether and 2mmol $Fe(acac)_3$. The reaction was stirred for 1 hour and heated to 260°C with reflux for 2 hours. The mixture was cooled to room temperature and mixed with 30 mL water. Insoluble materials were removed by centrifugation at 2,000xg for 30 minutes. The NPs were purified using magnetic (MACS) columns (Miltenyi Biotec, Auburn, CA, USA) and stored in water at room temperature or 4°C. The concentration of iron was determined spectrophotometrically at 410 nm in 2N hydrochloric acid (HCl).

pMHCII conjugation to NPs. pMHCII conjugation to maleimide-functionalized NPs (PFM) was done via the free C-terminal Cys engineered into the MHC chain/knob. Briefly, pMHCs were mixed with NPs in 40 mM phosphate buffer, pH 6.0, containing 2mM ethylenediaminetetraacetic acid (EDTA), 150mM NaCl, and incubated overnight at room temperature. pMHCII-conjugated NPs were purified by magnetic separation and concentrated by ultrafiltration through Amicon Ultra-15 (100 kDa cut-off) (Merck KGaA, Darmstadt, Germany) and stored in PBS.

NP characterization. The size and dispersity of unconjugated and pMHCII-conjugated NPs were assessed via transmission electron microscopy (TEM, Hitachi H7650, Hitachi, Chiyoda, Tokio, Japan) and dynamic light scattering (DLS, Zetasizer, Malvern Panalytical, Spectris, Egham, UK). Pegylated and pMHC-NPs were analyzed via 0.8% agarose gel electrophoresis, native- and denaturing 10% SDS-PAGE. To quantify pMHCII valency, we measured the pMHCII concentration of the pMHCII-NP preps using the Bradford assay (Thermo Scientific).

pMHCII-NP therapy of NOD mice. Cohorts of 10-week-old female NOD mice were injected i.v. with BDC2.5mi/IA^{g7}-coated NPs in PBS twice a week for 5 weeks. Treatment-induced formation and expansion of cognate Tetramer+ CD4+ T cells were assessed by flow cytometry.

CD4+ T cell samples used for next generation sequencing. Unless stated otherwise, NGS (next generation sequencing) data was obtained from non-restimulated BDC2.5/IA^{g7}-NP-induced CD4+ BDC2.5/IA^{g7}-Tetramer^{+} (CD4^{+}/B220^{-}/tet^{+}) T cells, Tconv (CD4^{+}/B220^{-}/tet^{-}) cells, also obtained from BDC2.5/IA^{g7}-NP-treated mice; KLH-DNP-immunized TFH (CD4^{+}/B220^{-}/CD44^{+}/PD1^{+}/CXCR5^{high}), and TH0 cells obtained from KLH-DNP-immunized mice (CD4^{+}/B220^{-}/CD44^{-}/PD1^{-}/CXCR5^{-}).

Bulk RNAseq. Cells were sorted in lysis buffer or PBS (5e4 cells) to perform RNA extractions for RNA sequencing (RNA-seq). For bulk RNAseq, we generated four independent samples containing tetramer^{+} and tetramer^{-} (Tconv) cells from two BDC2.5/IA^{g7}-NP-treated mice for each sample. For TFH and TH0 cells, we prepared RNA from three independent TFH cell pools (CD4^{+}/CD44^{hi}/CXCR5^{hi}/PD1^{hi}) and TH0 cells (CD4^{+}/CD44^{-}/CXCR5^{-}/PD1^{-}), as a negative control. All samples were coming from 3 immunized mice each.

Total RNA was prepared from sorted cells using the RNeasy Plus Mini Kit (Qiagen, Hilden, Germany) and used to prepare RNA-seq libraries and sequencing. Libraries were prepared using the TruSeq Stranded mRNA Sample Prep Kit v2 according to the manufacturer's protocol (Illumina, San Diego, CA, USA). Briefly, 10-50 ng of total RNA was used for poly(A)-mRNA purification using streptavidin-coated magnetic beads, followed by fragmentation to ~300bp. cDNA was synthesized using reverse transcriptase (SuperScript II, Invitrogen, Thermo Fisher Scientific, Waltham, MA, USA) and random primers. The second strand of the cDNA incorporated dUTP in place of dTTP. Double-stranded DNA was further used for library preparation. dsDNA was subjected to A-tailing and ligation of the barcoded Truseq adapters. All purification steps were performed using AMPure XP beads (Beckman Coulter, Brea, CA, USA). Library amplification was performed by PCR using the primer cocktail supplied in the kit. Final libraries were analyzed using Agilent DNA 1000 chip to estimate the quantity and size distribution. They were then quantified by qPCR using the KAPA Library Quantification Kit (Kapa Biosystems,

Roche, Basel, Switzerland) before amplification with Illumina's cBot. Libraries were loaded at a concentration of 2.75 pM onto the flowcell and sequenced 1 x 50 on Illumina's HiSeq 2500 to obtain 30-40M reads.

10X single-cell RNA-seq. At least 5e4 fresh, alive cells were collected in DMEM media (Sigma-Aldrich) supplemented with 10% FBS (Hyclone) at 4 ºC and sent to CNAG-CRG for processing and sequencing. In short, cells were separated into nanoscale gel beads emulsions with a 10X barcode. Cell numbers and viability were assessed using a TC20™ Automated Cell Counter (Bio-Rad Laboratories, Hercules, CA, USA), with a minimum target of 5000 cells. Later, cDNA sequencing libraries were produced using the NextGEM Single-cell 3' mRNA kit (v3.1; 10X Genomics) following the manufacturer's instructions. These steps involved GEM-RT clean-up, cDNA Amplification for 13 cycles, and cDNA quality control and quantification using the Agilent Bioanalyzer High Sensitivity chip (Agilent Technologies). Libraries were indexed by PCR using the PN-220103 Chromium i7 Sample Index Plate. Finally, sequencing was carried out on a NovaSeq 6000 sequencer (Illumina).

ATACseq. For ATAC-seq (Assay for Transposase-Accessible Chromatin using sequencing), 5e4 cells were sorted in PBS and processed for library preparation as described by (31). Briefly, cells were lysed in cold lysis buffer (10 mM Tris-HCl, pH 7.4,10 mM NaCl, 3 mM MgCl2, and 0.1% IGEPAL CA-630), washed, and right after resuspended in transposase reaction mix (25 µL 2x TD buffer, 2.5 µL transposase (Illumina) and 22.5 µL nuclease-free water) and incubated for 30 min at 37°C. Next, library fragments were amplified using 1x NEB Next PCR master mix (New England BioLabs) and 1.25 µM of custom Nextera PCR primers forward and reverse. Libraries were rendered using the barcoded primers Ad1_noMX as forward and Ad2.1-6 as reverse and purified using a PCR cleanup kit (Qiagen), yielding a final concentration of about 30 nM in 20 µL. Libraries were then analyzed on Bioanalyzer using an Agilent DNA High Sensitivity chip (Agilent

Technologies, Santa Clara, CA, USA) to estimate the quantity and size distribution. Next, they were quantified by qPCR using the KAPA Library Quantification Kit before amplification with Illumina's cBot. Libraries were finally loaded at 3.33 pM onto the flowcell and sequenced 1 x 50 on Illumina's HiSeq 2500.

10X single-cell multiome (scRNAseq+scATACseq). For 10X multiome RNA-seq+ATAC-seq, at least 5e5 fresh, alive cells were collected in DMEM media (Sigma-Aldrich) supplemented with 10% FBS (Hyclone) at 4 ºC, and then lysed and nuclei isolated. Nuclei were transposated and adapter sequences added to DNA fragments. Nuclei were then processed for single-cell barcoding and library generation following the manufacturer's instructions (CG000338; 10X Genomics). Briefly, isolated nuclei were partitioned into Gel Bead-In-Emulsions to produce barcoded cDNA from poly-adenylated mRNA as described above, as well as barcoded DNA fragments, and processed for library amplification and sequencing on a NovaSeq 6000 sequencer (Illumina) as described above

ChIP-seq. Chromatin immunoprecipitation (ChIP) and sequencing was performed for H3K4me3, H3K27me, and H3K27Ac bound DNA via ChIP-seq. We used 1e6 cells. Cells were pooled from tetramer+ T cells from BDC2.5/IA^{g7}-NP-treated mice (8 mice), and TFH (CD4^{+}/CD44^{hi}/CXCR5$^{hi/}$PD1^{hi}), and TH0 cells (CD4^{+}/CD44^{-}/CXCR5^{-}/PD1^{-}) (extract from the same group of 8 mice). In brief, cell dry pellets were fixed right after cell sorting with 10% PFA (paraformaldehyde) in DMEM (Sigma-Aldrich) supplemented with 10% FBS (Hyclone). Next, cells were lysed, sheared, and sonicated using an S220 Focused-ultrasonicator (Covaris, Woburn, MA, USA) (13 min, 105 W, 2% Duty Factor, 200 cycles). This was followed by overnight incubation with the precipitating antibody: 0.5 µL of H3K4me3 (Sigma), 0.5 µL of H3K27me3 (Cell Signaling, Danvers, Massachusetts, USA), and 2 µL of H3K27Ac (Abcam, Cambridge, United Carlsbad, CA, USA) and precipitated using Protein-A-Dynabeads (Abcam). RNA was cleared using RNAse A

(Qiagen) (1 h at 65 ºC), and decrosslinking was performed overnight with proteinase K at 65 ºC. DNA was finally purified with Phenol-Chloroform and EtOH-precipitation. After validation by Bioanalyzer analysis quality control (Agilent Technologies), samples were sequenced. Libraries were prepared using the NEB Next Ultra DNA Library Prep kit (Illumina) following the manufacturer's protocol. Libraries were loaded at a concentration of 2.75 pM onto flowcells and were sequenced 1 x 50 on Illumina's HiSeq 2500.

Methylome. For methylome analysis, genomic DNA was extracted using the DNeasy Blood and Tissue kit (Qiagen) following the manufacturer's instructions. Samples were then sent to Beijing Genomics Institute (BGI, Shenzhen, China), once frozen, for sequencing and bioinformatics analysis. DNA was processed by Whole Genome Bisulfite Sequencing (WGBS). DNA was sonicated to a mean size of 250 bp using a Bioruptor (Diagenode, Belgium) and ends blunted by dA addition to the 3'-end. Finally, adapters were ligated to protect bisulfite conversions. Next, ligated DNA was bisulfite converted using an EZ DNA Methylation-Gold kit (ZYMO, Irvine, CA, USA). Unmethylated cytosines were converted into uracil, which after purification and amplification via PCR, were converted back to thymine. Finally, samples were sequenced at 2x150 bp using NovaSeq 6000 system (Illumina).

Bioinformatic and statistical analyses. All fastq files obtained for each omics analysis were assessed for their quality control metrics before further downstream analysis using the FastQC tool. Sources for the indicated bioinformatic packages and tools are described further below.

RNA-seq. For bulk RNA-seq analysis, fastq file reads were aligned using STAR to GRCm38.p6 mouse genome, and gene counts were obtained using Gencode M25 annotation release version simultaneously with the "GeneCounts" STAR function. The resulting BAM files were processed into bigwig format for genomic tracks representation using samtools, deeptools, and trackViewer. Next, raw count values were processed and analyzed using R packages

DESeq2 for normalization, scaling, and negative binomial distribution differential analysis. ggplot2 (tidyverse) was mainly used for graphics rendering purposes. Differential analysis log2 fold changes results were shrunk using `apglm` to remove noise (57).

ATAC-seq and ChIP-seq. For bulk ATAC-seq analysis, Illumina adapters and low-quality bases were firstly removed from fastq files reads using Trimmomatic. Next, reads were aligned to GRCm38.p6 mouse genome using bowtie2, and duplicates were removed using Picard's `MarkDuplicates`. Then peaks were called using MACS2 with a q-value cutoff of 0.05, read extension of 5'->3' of 150, and keeping duplicates as they had been removed previously (`-q 0.05 --nomodel --extsize 150 --keep-dup all`). The resulting BAM files were processed into bigwig format for genomic tracks representation using samtools, deeptools, and trackViewer.

For ATAC-seq analysis differential open chromatin regions between samples were analyzed using DiffBind using BAM and peakset files. Briefly, we determined the overall background noise for each sample and then identified regions where the signal significantly exceeded noise, enabling accurate identification of peaks of enrichment controlling for false discovery rate (q-value < 0.05). Differential OCRs between cell types were determined using Likelihood Ratio (LR) to compare read counts or signal intensity within OCRs across samples.

Differential peaks between ChIPseq samples were obtained using GSA (Gene Set Analysis) from Partek®. Peaks were annotated using `annotatePeak` from the ChIPseeker package, using the UCSC mm10 reference included in org.Mm.eg.db and TxDb.Mmusculus.UCSC.mm10.knownGene R packages. Given that peak calling alone does not account for variations in the intensity of histone mark deposition, analysis of differential histone deposition includes both qualitative and quantitative assessments. Whereas qualitative assessment involves evaluating the overall pattern and distribution of the various histone marks, quantitative assessment measures the intensity and magnitude of histone mark deposition.

Methylome. Upstream bioinformatic analysis of whole-genome methylome data was performed by the bioinformatics team at BGI. In short, sequencing data was firstly filtered to

remove adaptor sequences and low-quality reads from raw reads. Filtered data was then mapped to the reference genome (mm10) by BSMAP, and duplication reads were removed. Regarding alignment quality metrics, the mapping rate and bisulfite conversion rate were measured for each sample. Only uniquely mapped data was used to get methylation data. Methylation level was determined by dividing the number of reads covering each mC by the total reads covering that cytosine. Differentially methylated regions (DMRs) were identified by comparison between sample methylomes using windows that contained at least 5 CpG (CHG or CHH) sites with at least a 2-fold change in methylation level and Fisher test p-value ≤ 0.05. Adjacent DMRs would be considered interdependent and joined into one continuous DMR if all the regions were differentially methylated between samples. Otherwise, DMRs were identified as independent. Genomic tracks for methylome data were represented using the trackViewer R package.

Single-cell RNAseq. 10X single-cell RNA-seq data was demultiplexed, aligned, and counts measured using Cellranger software from 10X Genomics. In short, Cellranger 10X software firstly filter and trim low-quality reads, then align them to a reference genome using STAR. Next, UMI (reads) and cell barcodes are filtered, grouped, and counted. Cells are called and reported their gene expression in matrices based on RNA content for each cell barcode. We then performed the secondary analysis of gene expression using the Seurat R package, where we firstly discarded poor quality cells based on features counts and mitochondrial and ribosomal content. Then, data was normalized, scaled, and dimensionally reduced using PCA (Principal Component Analysis) and UMAP (Uniform Manifold Approximation and Projection). Finally, cells were clustered using K-means, and visualization and differential analysis were performed.

Single-cell Multiome (scRNAseq+scATACseq). 10X single-cell multiomic data of simultaneous RNA-seq and ATAC-seq was analyzed using 10x Genomics software Cellranger-ARC. In this case, gene expression matrices from gene expression data are obtained like with Cellranger software (see the previous section). On the other hand, transposase accessibility data is adapter-removed and trimmed. Next, alignment is performed using the BWA-MEM algorithm,

using a fixed insert size distribution, and duplicates removed. Afterwards, peaks are called across all the cells to maximize the signal and then separated by barcode, obtaining peak-barcode matrices. Subsequently, gene expression and accessibility peaks matrices were combined and downstream-analyzed using Seurat and Signac packages. Like the scRNA-seq pipeline, data were first filtered for poor-quality cells using features and peaks counts, mitochondrial content, nucleosome signal, and transcription start site (TSS) enrichment. Later, RNA and ATAC data were normalized and scaled. Also, each dataset was dimensionally reduced using PCA for RNA and LSI (Latent Semantic Indexing) for ATAC and UMAP. Multidimensional reduction of joint RNA-seq and ATAC-seq data simultaneously was performed using the weighted-nearest neighbor (WNN) algorithm from Seurat and clustered using K-means.

Active enhancer prediction. ATAC-seq and H3K27ac-ChIPseq were used to predict potential active enhancer regions. Using the 'GenomicRanges' package, all peaks called for ATAC-seq overlapping peaks called for H3K27Ac deposition in the same sample, which were not in a promoter region (2 kb region upstream of TSS), were considered active enhancers.

Chromosome views. We used the trackViewer R package to combine the information from RNAseq, ATACseq, ChIPseq, predicted active enhancers and methylation data in linear plots representing gene tracks for specific genes. Alignment bam files for RNAseq, ATACseq and ChIPseq were transformed to BigWig format using deeptools.

Software and tools used for bioinformatic analyses. Bowtie2 (v2.4.2) (58); BSMAP (v3.0) (59); BWA (v0.0.7) (60); Cellranger (v6.0) (https://support.10xgenomics.com/single-cell-gene-expression/software/pipelines/latest/what-is-cell-ranger); Cellranger-arc (v2.0) (https://support.10xgenomics.com/single-cell-multiome-atac-gex/software/pipelines/latest/what-is-cell-ranger-arc); ChipSeeker (v1.28.3) (61); clusterProfiler (v4.0.5) (62) Deeptools (v3.5.0) (63); Deseq2 (v1.32.0) (64); DiffBind (v3.2.7) (65); FastQC (http://www.bioinformatics.babraham.ac.uk/projects/fastqc/); FlowJo v9 (https://www.flowjo.com);

Genomic Ranges (v1.44.0) (66); MACS2 (v2.2.7.1) (67); org.Mm.eg.db (v3.13.0) (https://bioconductor.org/packages/release/data/annotation/html/ org.Mm.eg.db.html); Partek® Flow® software (https://www.partek.com/partek-flow/); Picard (v2.25.0) (https://broadinstitute.github.io/picard/); R (v4.1.0), R Core Team (2020). — European Environment Agency, n.d.) (https://www.eea.europa.eu/data-and-maps/indicators/oxygen-consuming-substances-in-rivers/r-development-core-team-2006); Rstudio (v1.4.1103) (https://www.rstudio.com/); Samtools (68); Seurat (v4.0.3) (69); Signac (v1.3.0) (70); STAR (v2.7.10a) (71); Tidyverse (v1.3.1) (https://www.tidyverse.org); Trackviewer (v1.31.1) (72); Trimmomatic (v.039) (73).

Statistical analyses. Statistical significance of the transcriptomic and epigenetic data was compared using the bioinformatic tools described above. Statistical significance for differences in the numbers of genes shared between different subsets was determined using the Chi-Square test.

Data and code availability: The raw and processed data supporting the findings of this study are available at the Gene Expression Omnibus (GEO) database. Accession numbers are as follows: GSE173681 (bulk RNA-seq data); GSE182636 (scRNA-seq data); and GSE248152 (ATAC-seq, ChIP-seq, methylome, and single-cell multiome data).

Acknowledgments

We thank S. Thiessen, J. Erickson, J. Fetsch, G. Mendizabal, F. Liu for technical contributions and/or animal care, Y. Liu for flow cytometry, K. Poon from the Nicole Perkins Microbial Communities Core for flow cytometry, P. Nieto, E. Mereu, G. Lunazzi and H. Heyn from the Centre Nacional d'Anàlisi Genòmica (CNAG), I. González and F. Fernández from the Centre for Genomic Regulation (CRG), and S. Wegener from the University of Calgary's Center for Health Genomics and Informatics, for library preparation and/or sequencing. This work was supported by Genome Canada and Genome Alberta (GAPP program), the Canadian Institutes of Health Research (CIHR) (FDN-353029, PJT-479040, PJT-479038, FRN-168480 (with JDRF), DT4-179512), the Praespero Foundation, the ISCIII and FEDER (PIE14/00027, PI15/0797), Ministerio de Ciencia e Innovación of Spain (MCIN; PID2021-125493OB-I00), Generalitat de Catalunya (SGR and CERCA Programmes) and Red Española de Supercomputación (RES, providing CSUC resources). J. Garnica and P. Solé were supported by a predoctoral studentship from FPU (MCIN). P. Serra was an investigator of the Ramon y Cajal re-integration program and was supported by a JDRF Career Development Award.

Author contributions

P. Solé generated the data for Figs. 2, 4, 5, 6 and 7 with contributions from C.F. and J.Y. J.G. generated the data for Figs. 1 and 3 and analyzed all the datasets bioinformatically to generate Figs. 1-7, and Suppl. Figs. 1-3 with contributions from J.M. J.M. generated Fig. 5 and Suppl. Figs. 5-7. D.M. produced pMHCII-NP and pMHCII tetramers. P. Serra co-supervised IDIBAPS co-authors with P. Santamaria. P. Santamaria designed the study, supervised its execution and wrote the manuscript with J. Garnica.

Competing interests

P. Santamaria is founder, scientific officer and stockholder of Parvus Therapeutics. He is inventor on patents on pMHC-based nanomedicines and receives funding from the company. He also has a consulting agreement with Sanofi. The other authors declare no competing interests.

References

1. Roncarolo MG, Gregori S, Bacchetta R, Battaglia M, Gagliani N. The Biology of T Regulatory Type 1 Cells and Their Therapeutic Application in Immune-Mediated Diseases. Immunity. 2018;49(6):1004-19.
2. Singha S, Shao K, Yang Y, Clemente-Casares X, Sole P, Clemente A, et al. Peptide-MHC-based nanomedicines for autoimmunity function as T-cell receptor microclustering devices. Nature nanotechnology. 2017;12(7):701-10.
3. Clemente-Casares X, Blanco J, Ambalavalan P, Yamanouchi J, Singha S, Fandos C, et al. Expanding antigen-specific regulatory networks to treat autoimmunity. Nature. 2016;530(7591):434-40.
4. Umeshappa CS, Mbongue J, Singha S, Mohapatra S, Yamanouchi J, Lee JA, et al. Ubiquitous antigen-specific T regulatory type 1 cells variably suppress hepatic and extrahepatic autoimmunity. J Clin Invest. 2020;130(4):1823-9.
5. Umeshappa CS, Singha S, Blanco J, Shao K, Nanjundappa RH, Yamanouchi J, et al. Suppression of a broad spectrum of liver autoimmune pathologies by single peptide-MHC-based nanomedicines. Nature communications. 2019;10(1):2150.
6. Sole P, Yamanouchi J, Garnica J, Uddin MM, Clarke R, Moro J, et al. A T follicular helper cell origin for T regulatory type 1 cells. Cell Mol Immunol. 2023;20(5):489-511.
7. Sole P, Parras D, Yamanouchi J, Garnica J, Garabatos N, Moro J, et al. Transcriptional re-programming of insulin B-chain epitope-specific T-follicular helper cells into anti-diabetogenic T-regulatory type-1 cells. Front Immunol. 2023;14:1177722.
8. O'Garra A, Arai N. The molecular basis of T helper 1 and T helper 2 cell differentiation. Trends Cell Biol. 2000;10(12):542-50.

9. Avni O, Lee D, Macian F, Szabo SJ, Glimcher LH, Rao A. T(H) cell differentiation is accompanied by dynamic changes in histone acetylation of cytokine genes. Nat Immunol. 2002;3(7):643-51.
10. Ostuni R, Piccolo V, Barozzi I, Polletti S, Termanini A, Bonifacio S, et al. Latent enhancers activated by stimulation in differentiated cells. Cell. 2013;152(1-2):157-71.
11. Belk JA, Yao W, Ly N, Freitas KA, Chen YT, Shi Q, et al. Genome-wide CRISPR screens of T cell exhaustion identify chromatin remodeling factors that limit T cell persistence. Cancer Cell. 2022;40(7):768-86 e7.
12. Hatton RD, Harrington LE, Luther RJ, Wakefield T, Janowski KM, Oliver JR, et al. A distal conserved sequence element controls Ifng gene expression by T cells and NK cells. Immunity. 2006;25(5):717-29.
13. Schoenborn JR, Dorschner MO, Sekimata M, Santer DM, Shnyreva M, Fitzpatrick DR, et al. Comprehensive epigenetic profiling identifies multiple distal regulatory elements directing transcription of the gene encoding interferon-gamma. Nat Immunol. 2007;8(7):732-42.
14. Jones B, Chen J. Inhibition of IFN-gamma transcription by site-specific methylation during T helper cell development. EMBO J. 2006;25(11):2443-52.
15. Chang S, Aune TM. Dynamic changes in histone-methylation 'marks' across the locus encoding interferon-gamma during the differentiation of T helper type 2 cells. Nat Immunol. 2007;8(7):723-31.
16. Koyanagi M, Baguet A, Martens J, Margueron R, Jenuwein T, Bix M. EZH2 and histone 3 trimethyl lysine 27 associated with Il4 and Il13 gene silencing in Th1 cells. J Biol Chem. 2005;280(36):31470-7.
17. Akimzhanov AM, Yang XO, Dong C. Chromatin remodeling of interleukin-17 (IL-17)-IL-17F cytokine gene locus during inflammatory helper T cell differentiation. J Biol Chem. 2007;282(9):5969-72.

18. Fann M, Godlove JM, Catalfamo M, Wood WH, 3rd, Chrest FJ, Chun N, et al. Histone acetylation is associated with differential gene expression in the rapid and robust memory CD8(+) T-cell response. Blood. 2006;108(10):3363-70.
19. Araki Y, Wang Z, Zang C, Wood WH, 3rd, Schones D, Cui K, et al. Genome-wide analysis of histone methylation reveals chromatin state-based regulation of gene transcription and function of memory CD8+ T cells. Immunity. 2009;30(6):912-25.
20. Teghanemt A, Pulipati P, Misel-Wuchter K, Day K, Yorek MS, Yi R, et al. CD4 expression in effector T cells depends on DNA demethylation over a developmentally established stimulus-responsive element. Nature communications. 2022;13(1):1477.
21. Fields PE, Lee GR, Kim ST, Bartsevich VV, Flavell RA. Th2-specific chromatin remodeling and enhancer activity in the Th2 cytokine locus control region. Immunity. 2004;21(6):865-76.
22. Lee DU, Agarwal S, Rao A. Th2 lineage commitment and efficient IL-4 production involves extended demethylation of the IL-4 gene. Immunity. 2002;16(5):649-60.
23. Kim ST, Fields PE, Flavell RA. Demethylation of a specific hypersensitive site in the Th2 locus control region. Proc Natl Acad Sci U S A. 2007;104(43):17052-7.
24. Liu X, Lu H, Chen T, Nallaparaju KC, Yan X, Tanaka S, et al. Genome-wide Analysis Identifies Bcl6-Controlled Regulatory Networks during T Follicular Helper Cell Differentiation. Cell Rep. 2016;14(7):1735-47.
25. Liu B, Tahk S, Yee KM, Fan G, Shuai K. The ligase PIAS1 restricts natural regulatory T cell differentiation by epigenetic repression. Science. 2010;330(6003):521-5.
26. Ohkura N, Hamaguchi M, Morikawa H, Sugimura K, Tanaka A, Ito Y, et al. T cell receptor stimulation-induced epigenetic changes and Foxp3 expression are independent and complementary events required for Treg cell development. Immunity. 2012;37(5):785-99.
27. Durek P, Nordstrom K, Gasparoni G, Salhab A, Kressler C, de Almeida M, et al. Epigenomic Profiling of Human CD4(+) T Cells Supports a Linear Differentiation Model and Highlights Molecular Regulators of Memory Development. Immunity. 2016;45(5):1148-61.

28. Holliday R, Pugh JE. DNA modification mechanisms and gene activity during development. Science. 1975;187(4173):226-32.
29. Muramoto T, Muller I, Thomas G, Melvin A, Chubb JR. Methylation of H3K4 Is required for inheritance of active transcriptional states. Curr Biol. 2010;20(5):397-406.
30. Raas MWD, Zijlmans DW, Vermeulen M, Marks H. There is another: H3K27me3-mediated genomic imprinting. Trends Genet. 2022;38(1):82-96.
31. Buenrostro JD, Giresi PG, Zaba LC, Chang HY, Greenleaf WJ. Transposition of native chromatin for fast and sensitive epigenomic profiling of open chromatin, DNA-binding proteins and nucleosome position. Nat Methods. 2013;10(12):1213-8.
32. Greer EL, Shi Y. Histone methylation: a dynamic mark in health, disease and inheritance. Nat Rev Genet. 2012;13(5):343-57.
33. Creyghton MP, Cheng AW, Welstead GG, Kooistra T, Carey BW, Steine EJ, et al. Histone H3K27ac separates active from poised enhancers and predicts developmental state. Proc Natl Acad Sci U S A. 2010;107(50):21931-6.
34. Jadhav U, Nalapareddy K, Saxena M, O'Neill NK, Pinello L, Yuan GC, et al. Acquired Tissue-Specific Promoter Bivalency Is a Basis for PRC2 Necessity in Adult Cells. Cell. 2016;165(6):1389-400.
35. Schubeler D. Function and information content of DNA methylation. Nature. 2015;517(7534):321-6.
36. Barnett KR, Decato BE, Scott TJ, Hansen TJ, Chen B, Attalla J, et al. ATAC-Me Captures Prolonged DNA Methylation of Dynamic Chromatin Accessibility Loci during Cell Fate Transitions. Mol Cell. 2020.
37. Heintzman ND, Stuart RK, Hon G, Fu Y, Ching CW, Hawkins RD, et al. Distinct and predictive chromatin signatures of transcriptional promoters and enhancers in the human genome. Nat Genet. 2007;39(3):311-8.

38. Rada-Iglesias A, Bajpai R, Swigut T, Brugmann SA, Flynn RA, Wysocka J. A unique chromatin signature uncovers early developmental enhancers in humans. Nature. 2011;470(7333):279-83.
39. Pekowska A, Benoukraf T, Zacarias-Cabeza J, Belhocine M, Koch F, Holota H, et al. H3K4 tri-methylation provides an epigenetic signature of active enhancers. EMBO J. 2011;30(20):4198-210.
40. Schlesinger F, Smith AD, Gingeras TR, Hannon GJ, Hodges E. De novo DNA demethylation and noncoding transcription define active intergenic regulatory elements. Genome Res. 2013;23(10):1601-14.
41. Stadler MB, Murr R, Burger L, Ivanek R, Lienert F, Scholer A, et al. DNA-binding factors shape the mouse methylome at distal regulatory regions. Nature. 2011;480(7378):490-5.
42. Ciofani M, Madar A, Galan C, Sellars M, Mace K, Pauli F, et al. A validated regulatory network for Th17 cell specification. Cell. 2012;151(2):289-303.
43. Li P, Spolski R, Liao W, Wang L, Murphy TL, Murphy KM, et al. BATF-JUN is critical for IRF4-mediated transcription in T cells. Nature. 2012;490(7421):543-6.
44. Xu W, Zhao X, Wang X, Feng H, Gou M, Jin W, et al. The Transcription Factor Tox2 Drives T Follicular Helper Cell Development via Regulating Chromatin Accessibility. Immunity. 2019;51(5):826-39 e5.
45. Crotty S, Johnston RJ, Schoenberger SP. Effectors and memories: Bcl-6 and Blimp-1 in T and B lymphocyte differentiation. Nat Immunol. 2010;11(2):114-20.
46. Chihara N, Madi A, Kondo T, Zhang H, Acharya N, Singer M, et al. Induction and transcriptional regulation of the co-inhibitory gene module in T cells. Nature. 2018;558(7710):454-9.
47. Miraldi ER, Pokrovskii M, Watters A, Castro DM, De Veaux N, Hall JA, et al. Leveraging chromatin accessibility for transcriptional regulatory network inference in T Helper 17 Cells. Genome Res. 2019;29(3):449-63.

48. Wei L, Vahedi G, Sun HW, Watford WT, Takatori H, Ramos HL, et al. Discrete roles of STAT4 and STAT6 transcription factors in tuning epigenetic modifications and transcription during T helper cell differentiation. Immunity. 2010;32(6):840-51.
49. Pot C, Apetoh L, Awasthi A, Kuchroo VK. Induction of regulatory Tr1 cells and inhibition of T(H)17 cells by IL-27. Semin Immunol. 2011;23(6):438-45.
50. Lu KT, Kanno Y, Cannons JL, Handon R, Bible P, Elkahloun AG, et al. Functional and epigenetic studies reveal multistep differentiation and plasticity of in vitro-generated and in vivo-derived follicular T helper cells. Immunity. 2011;35(4):622-32.
51. Wei G, Wei L, Zhu J, Zang C, Hu-Li J, Yao Z, et al. Global mapping of H3K4me3 and H3K27me3 reveals specificity and plasticity in lineage fate determination of differentiating CD4+ T cells. Immunity. 2009;30(1):155-67.
52. Gounari F, Khazaie K. TCF-1: a maverick in T cell development and function. Nat Immunol. 2022;23(5):671-8.
53. Wang W, Chandra A, Goldman N, Yoon S, Ferrari EK, Nguyen SC, et al. TCF-1 promotes chromatin interactions across topologically associating domains in T cell progenitors. Nat Immunol. 2022;23(7):1052-62.
54. Zhong Y, Walker SK, Pritykin Y, Leslie CS, Rudensky AY, van der Veeken J. Hierarchical regulation of the resting and activated T cell epigenome by major transcription factor families. Nat Immunol. 2022;23(1):122-34.
55. Umeshappa CS, Sole P, Yamanouchi J, Mohapatra S, Surewaard BGJ, Garnica J, et al. Re-programming mouse liver-resident invariant natural killer T cells for suppressing hepatic and diabetogenic autoimmunity. Nature communications. 2022;13(1):3279.
56. Serra P, Garabatos N, Singha S, Fandos C, Garnica J, Sole P, et al. Increased yields and biological potency of knob-into-hole-based soluble MHC class II molecules. Nature communications. 2019;10(1):4917.

57. Zhu A, Ibrahim JG, Love MI. Heavy-tailed prior distributions for sequence count data: removing the noise and preserving large differences. Bioinformatics. 2019;35(12):2084-92.
58. Langmead B, Salzberg SL. Fast gapped-read alignment with Bowtie 2. Nat Methods. 2012;9(4):357-9.
59. Xi Y, Li W. BSMAP: whole genome bisulfite sequence MAPping program. BMC Bioinformatics. 2009;10:232.
60. Li H, Durbin R. Fast and accurate long-read alignment with Burrows-Wheeler transform. Bioinformatics. 2010;26(5):589-95.
61. Yu G, Wang LG, He QY. ChIPseeker: an R/Bioconductor package for ChIP peak annotation, comparison and visualization. Bioinformatics. 2015;31(14):2382-3.
62. Wu T, Hu E, Xu S, Chen M, Guo P, Dai Z, et al. clusterProfiler 4.0: A universal enrichment tool for interpreting omics data. Innovation (Camb). 2021;2(3):100141.
63. Ramirez F, Dundar F, Diehl S, Gruning BA, Manke T. deepTools: a flexible platform for exploring deep-sequencing data. Nucleic Acids Res. 2014;42(Web Server issue):W187-91.
64. Love MI, Huber W, Anders S. Moderated estimation of fold change and dispersion for RNA-seq data with DESeq2. Genome Biol. 2014;15(12):550.
65. Ross-Innes CS, Stark R, Teschendorff AE, Holmes KA, Ali HR, Dunning MJ, et al. Differential oestrogen receptor binding is associated with clinical outcome in breast cancer. Nature. 2012;481(7381):389-93.
66. Lawrence M, Huber W, Pages H, Aboyoun P, Carlson M, Gentleman R, et al. Software for computing and annotating genomic ranges. PLoS Comput Biol. 2013;9(8):e1003118.
67. Zhang Y, Liu T, Meyer CA, Eeckhoute J, Johnson DS, Bernstein BE, et al. Model-based analysis of ChIP-Seq (MACS). Genome Biol. 2008;9(9):R137.
68. Li H, Handsaker B, Wysoker A, Fennell T, Ruan J, Homer N, et al. The Sequence Alignment/Map format and SAMtools. Bioinformatics. 2009;25(16):2078-9.

69. Hao Y, Hao S, Andersen-Nissen E, Mauck WM, 3rd, Zheng S, Butler A, et al. Integrated analysis of multimodal single-cell data. Cell. 2021;184(13):3573-87 e29.
70. Stuart T, Srivastava A, Madad S, Lareau CA, Satija R. Single-cell chromatin state analysis with Signac. Nat Methods. 2021;18(11):1333-41.
71. Dobin A, Davis CA, Schlesinger F, Drenkow J, Zaleski C, Jha S, et al. STAR: ultrafast universal RNA-seq aligner. Bioinformatics. 2013;29(1):15-21.
72. Ou J, Zhu LJ. trackViewer: a Bioconductor package for interactive and integrative visualization of multi-omics data. Nat Methods. 2019;16(6):453-4.
73. Bolger AM, Lohse M, Usadel B. Trimmomatic: a flexible trimmer for Illumina sequence data. Bioinformatics. 2014;30(15):2114-20.

Fig. 1

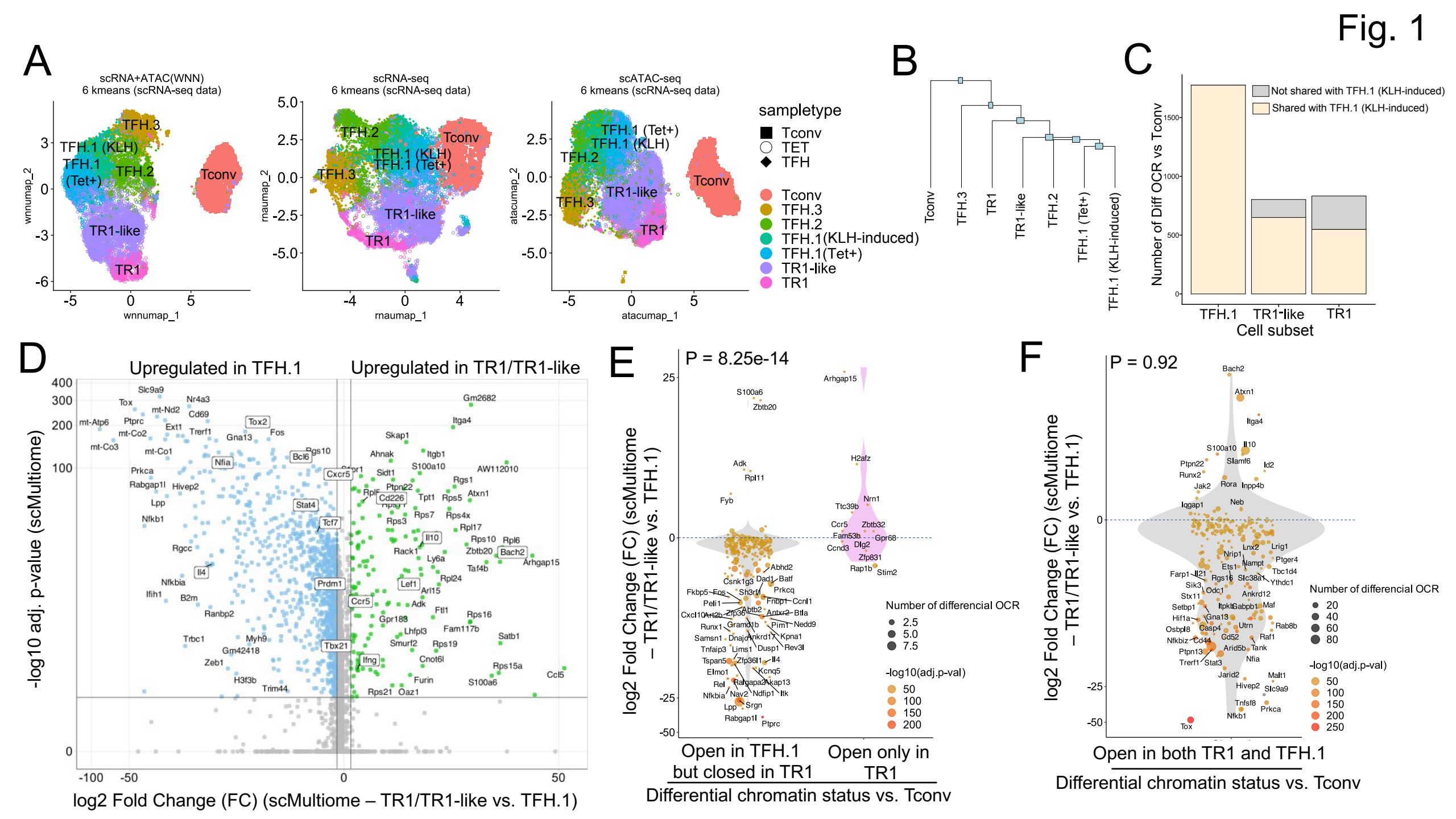
A
scRNA+ATAC(WNN)
6 kmeans (scRNA-seq data)
scRNA-seq
6 kmeans (scRNA-seq data)
scATAC-seq
6 kmeans (scRNA-seq data)
TFH.3
TFH.1 (KLH)
TFH.1 (Tet+)
TFH.2
Tconv
TR1-like
TR1
wnnumap_1
wnnumap_2
rnaumap_1
rnaumap_2
atacumap_1
atacumap_2
sampletype
Tconv
TET
TFH
Tconv
TFH.3
TFH.2
TFH.1(KLH-induced)
TFH.1(Tet+)
TR1-like
TR1
B
Tconv
TFH.3
TR1
TR1-like
TFH.2
TFH.1 (Tet+)
TFH.1 (KLH-induced)
C
Not shared with TFH.1 (KLH-induced)
Shared with TFH.1 (KLH-induced)
Number of Diff OCR vs Tconv
TFH.1
TR1-like
TR1
Cell subset
D
Upregulated in TFH.1
Upregulated in TR1/TR1-like
-log10 adj. p-value (scMultiome)
log2 Fold Change (FC) (scMultiome – TR1/TR1-like vs. TFH.1)
E
P = 8.25e-14
log2 Fold Change (FC) (scMultiome – TR1/TR1-like vs. TFH.1)
Number of differencial OCR
-log10(adj.p-val)
Open in TFH.1 but closed in TR1
Open only in TR1
Differential chromatin status vs. Tconv
F
P = 0.92
log2 Fold Change (FC) (scMultiome – TR1/TR1-like vs. TFH.1)
Number of differencial OCR
-log10(adj.p-val)
Open in both TR1 and TFH.1
Differential chromatin status vs. Tconv

Figure 1. The TFH-to-TR1 conversion is associated with massive closure of previously open chromatin regions and gene silencing.

BDC2.5mi/I-A^{g7}-NP-induced Tet+ (TET); KLH-DNP-induced TFH (TFH), and Tconv cells (Tconv) from female NOD mice (n=4, 8 and 1 mice, respectively) were sorted and processed for 10X GEX+ATAC multiome. (**A**) Left: multidimensional analysis of scRNAseq and ATACseq data using weighted nearest neighbor (WNN). Cell type prediction is based on K-means clusterization and predicted cell subtype classification of scRNAseq data. Middle and right: scRNAseq (middle) and scATACseq (right) UMAP plots with K-means clusterization and predicted cell subtype classification based on scRNAseq data. The legends' colors correspond to different T cell types and the legends' shape correspond to sample type. (**B**) Hierarchical clustering of multiome data based on Euclidean distance of all the clusters found in all sample types. (**C**) Bar plot with the number of differentially open chromatin regions in TFH.1 (including Tet+ TFH.1 and KLH-DNP-induced TFH.1 cells), TR1/TR1-like cells, as compared to Tconv cells (adjusted P <0.05). Color depicts the proportion of OCRs that are shared with KLH-DNP-induced TFH.1 (vs Tconv cells) (yellow) or that appear *de novo* in TR1/TR1-like cells (grey). **(D**) Volcano plot of Wilcox's differential analysis of scRNAseq data from the multiome dataset comparing TFH.1 and TR1/TR1-like cells. Not overlapping dots were labelled. Genes mentioned in the text are boxed. (**E-F**) Jitter plots depicting log2FC in gene expression between TR1/TR1-like and TFH.1 cells as measured by scRNAseq (adjusted P<0.05) for genes associated with OCRs found in TFH.1 cells (left; closed in TR1/TR1-like cells) or TR1/TR1-like (right; closed in TFH.1 cells) (**E**), or in both TFH.1 and TR1/TR1-like cells (**F**) as measured by scATACseq (adjusted P<0.05). Dot (gene) colors define the -log10 (adjusted P) for RNA expression of Wilcox test; dot sizes are proportional to the number of differential OCRs associated with each gene. All genes are labelled except when overlapping. Chromatin closure by TR1 cells was significantly associated with gene downregulation as determined via Chi-square test.

Fig. 2

A

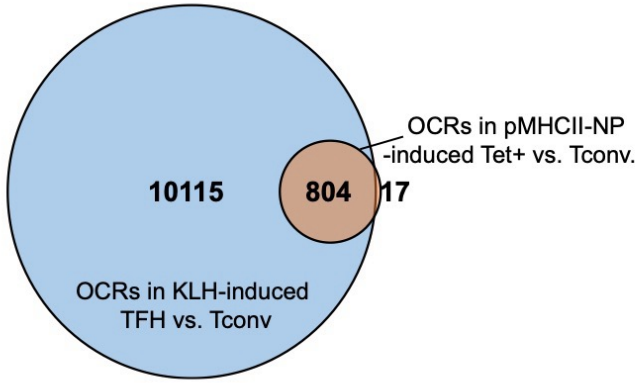
10115
804
17
OCRs in pMHCII-NP -induced Tet+ vs. Tconv.
OCRs in KLH-induced TFH vs. Tconv

B

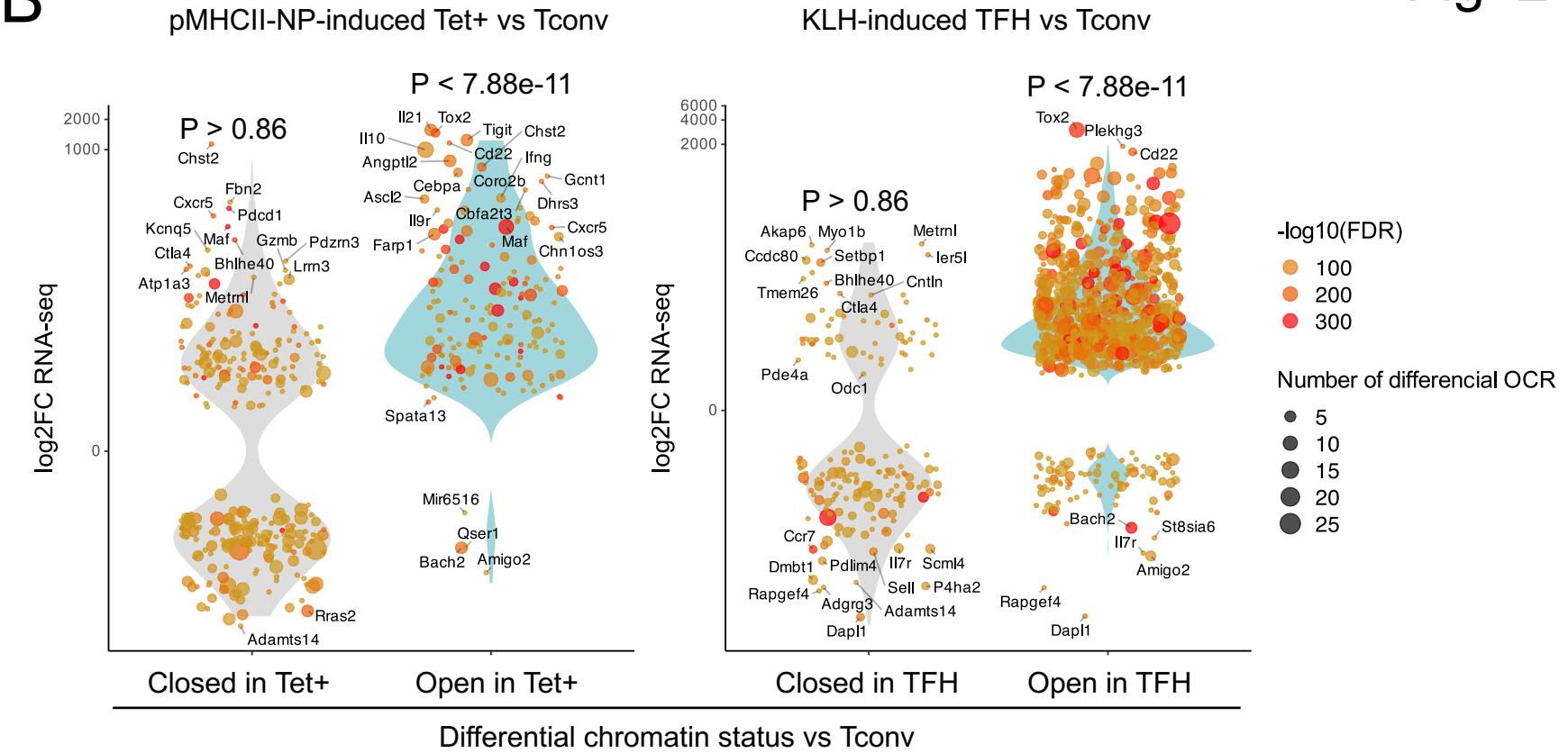
pMHCII-NP-induced Tet+ vs Tconv
KLH-induced TFH vs Tconv
P < 7.88e-11
P > 0.86
log2FC RNA-seq
Chst2
Fbn2
Cxcr5
Pdcd1
Kcnq5
Maf
Gzmb
Pdzrn3
Ctla4
Bhlhe40
Lrrn3
Atp1a3
Metrnl
Rras2
Adamts14
Il21
Tox2
Il10
Tigit
Chst2
Angptl2
Cd22
Ifng
Cebpa
Coro2b
Gcnt1
Ascl2
Dhrs3
Il9r
Cbfa2t3
Cxcr5
Farp1
Maf
Chn1os3
Spata13
Mir6516
Qser1
Bach2
Amigo2
Akap6
Myo1b
Metrnl
Ccdc80
Setbp1
Ier5l
Tmem26
Bhlhe40
Cntln
Ctla4
Pde4a
Odc1
Ccr7
Dmbt1
Pdlim4
Il7r
Scml4
Sell
P4ha2
Rapgef4
Adgrg3
Adamts14
Dapl1
Tox2
Plekhg3
Cd22
Bach2
St8sia6
Il7r
Amigo2
Rapgef4
Dapl1
-log10(FDR)
100
200
300
Number of differencial OCR
5
10
15
20
25
Closed in Tet+
Open in Tet+
Closed in TFH
Open in TFH
Differential chromatin status vs Tconv

C

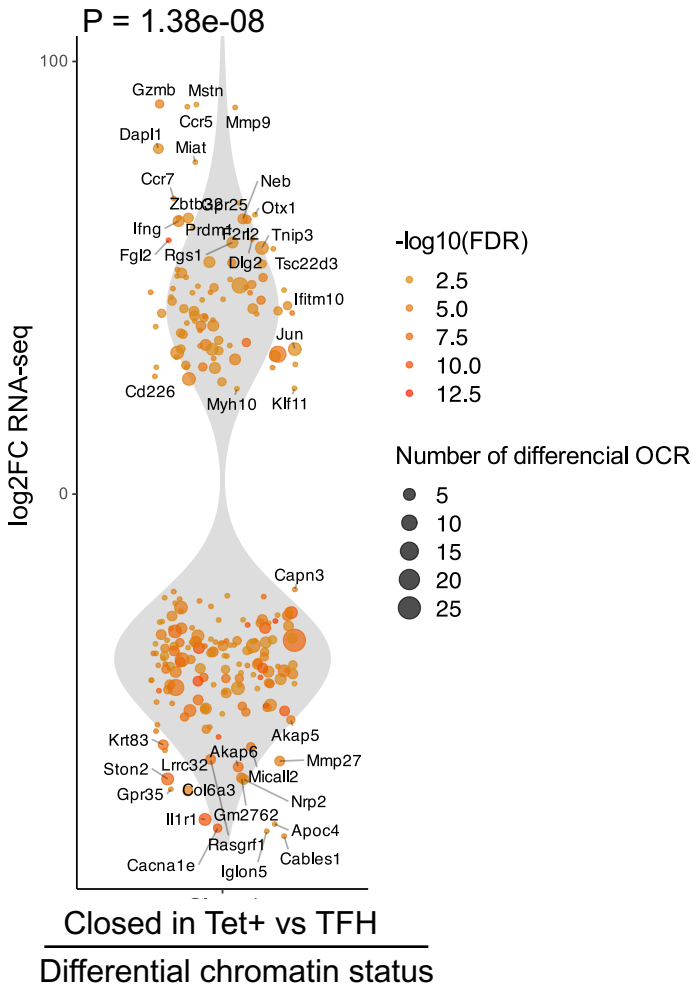
P = 1.38e-08
log2FC RNA-seq
Gzmb
Mstn
Ccr5
Mmp9
Dapl1
Miat
Ccr7
Neb
Zbtb32
Gpr25
Otx1
Ifng
Prdm1
Il2rl2
Tnip3
Fgl2
Rgs1
Dlg2
Tsc22d3
Ifitm10
Jun
Cd226
Myh10
Klf11
Capn3
Krt83
Akap5
Ston2
Lrrc32
Akap6
Mmp27
Micall2
Gpr35
Col6a3
Nrp2
Il1r1
Gm2762
Apoc4
Rasgrf1
Cacna1e
Iglon5
Cables1
-log10(FDR)
2.5
5.0
7.5
10.0
12.5
Number of differencial OCR
5
10
15
20
25
Closed in Tet+ vs TFH
Differential chromatin status

Figure 2. Chromatin accessibility in BDC2.5mi/I-A^{g7}-NP-induced Tet+ and KLH-DNP-induced TFH cells versus gene expression.

(**A**) Euler's plot comparing the number and sharing of differential OCRs between BDC2.5mi/I-A^{g7}-NP-induced Tet+ and KLH-induced TFH cells relative to their Tconv counterparts (n=4, 3 and 3, respectively) (adjusted P<0.01). (**B**) Associations between the number and status of differentially open or closed chromatin sites and gene expression as measured via bulk ATACseq (adjusted P<0.01) and RNAseq (adjusted P<0.01 and |log2FC|>2), respectively. Data correspond, from left to right, to BDC2.5mi/I-A^{g7}-NP-induced Tet+ vs Tconv and KLH-induced TFH vs Tconv. Each dot represents a gene, and its size is proportional to the number of associated OCRs. Dot color represents RNAseq differential analysis' -log10 of False Discovery Rate (FDR). Only genes with the highest log2FC value in each condition were labelled. (**C**) Associations between the status of chromatin accessibility in BDC2.5mi/I-A^{g7}-NP-induced Tet+ vs. KLH-induced TFH cells and gene expression as measured via bulk ATACseq (adjusted P<0.01) and RNAseq (adjusted P<0.01 and |log2FC|>2), respectively. Each dot represents a gene, and its size is proportional to the number of associated OCRs. Dot color represents RNAseq differential analysis' -log10 of False Discovery Rate (FDR). Only genes with the highest log2FC value in each condition were labelled. P values in (**B**) and (**C**) were calculated using Chi-square.

Fig. 3

A

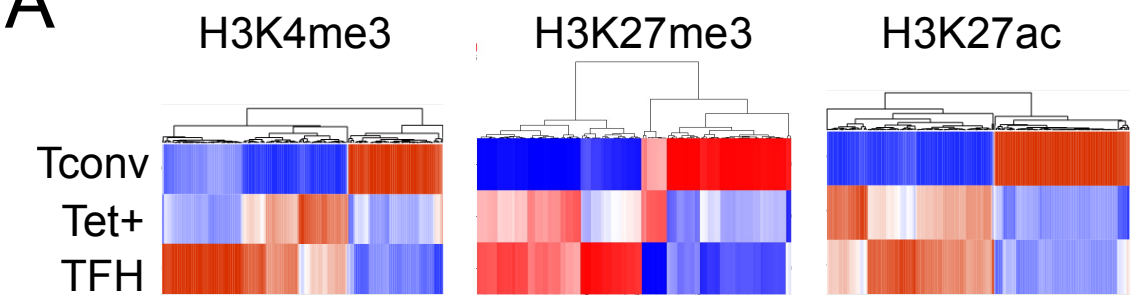
H3K4me3
H3K27me3
H3K27ac
Tconv
Tet+
TFH

B

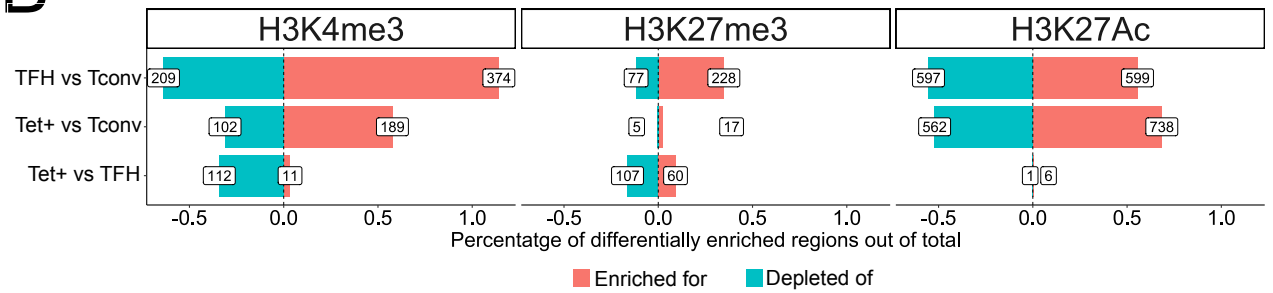
H3K4me3
H3K27me3
H3K27Ac
TFH vs Tconv
Tet+ vs Tconv
Tet+ vs TFH
209
374
77
228
597
599
102
189
5
17
562
738
112
11
107
60
1
6
-0.5
0.0
0.5
1.0
Percentatge of differentially enriched regions out of total
Enriched for
Depleted of

Figure 3. Genome-wide distribution of H3K4me3, H3K27me3, and H3K27ac marks and active enhancers in BDC2.5mi/I-A^{g7}-NP-induced Tet+ cells and KLH-DNP-induced TFH cells versus differential gene expression.

(**A**) Clustering heatmaps of all the regions enriched for H3K4me3 (top), H3K27me3 (middle) and H3K27Ac (bottom) deposition in BDC2.5mi/I-A^{g7}-NP-induced Tet+ cells, KLH-DNP-induced TFH cells and Tconv cells. The intensity of the red color is proportional to the magnitude of enrichment vs. the corresponding background. (**B**) Bar plot comparing the relative percentages (X axis) and absolute numbers (number annotations in each bar) of differentially marked regions for each histone modification (FDR<0.01). Top, middle and bottom rows correspond to KLH-DNP-induced TFH vs Tconv, BDC2.5mi/I-A^{g7}-NP-induced Tet+ vs Tconv and BDC2.5mi/I-A^{g7}-NP-induced Tet+ vs KLH-DNP-induced TFH comparisons, respectively.

Fig. 4

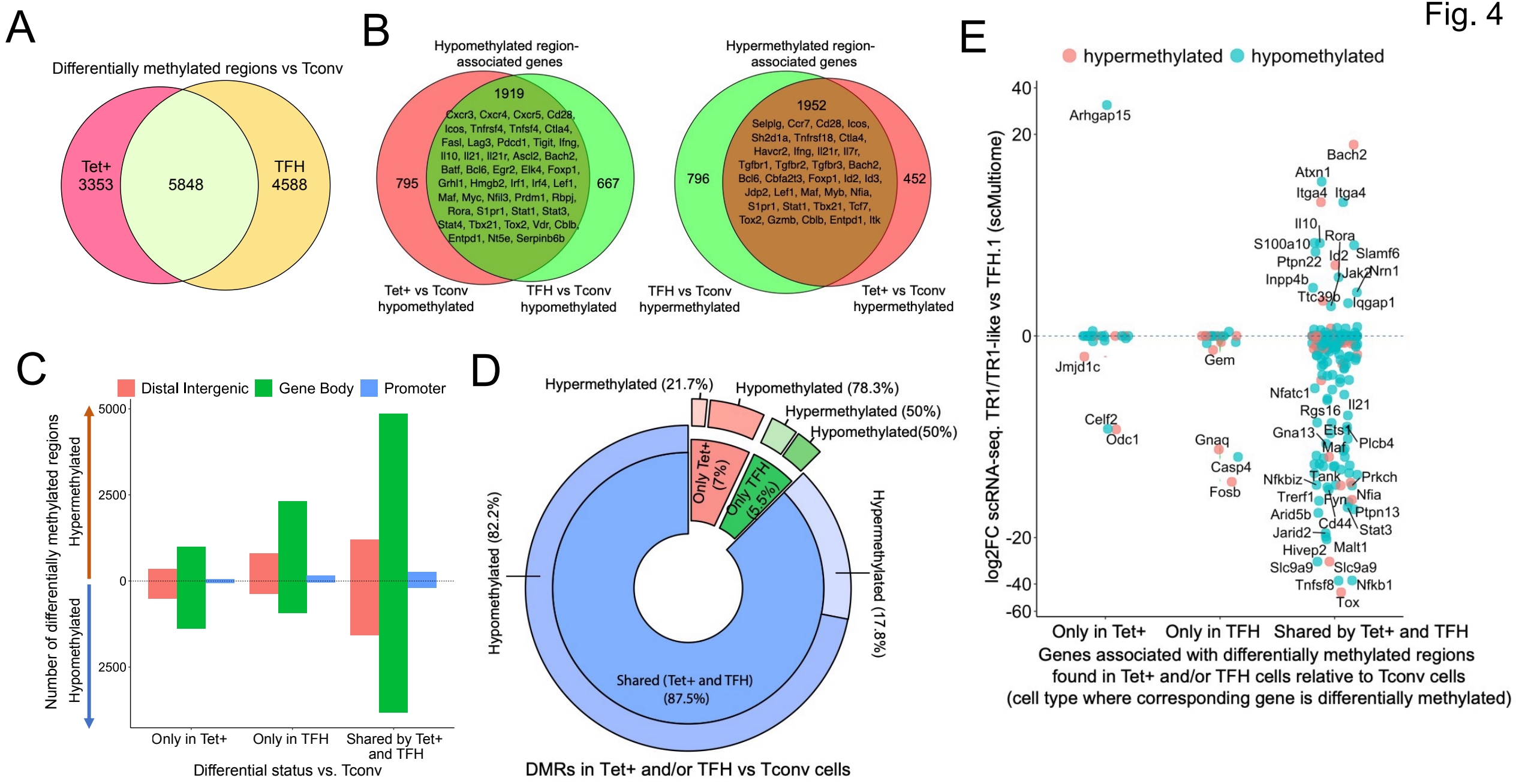
A
Differentially methylated regions vs Tconv
Tet+
3353
5848
TFH
4588
B
Hypomethylated region-associated genes
1919
Cxcr3, Cxcr4, Cxcr5, Cd28, Icos, Tnfrsf4, Tnfsf4, Ctla4, Fasl, Lag3, Pdcd1, Tigit, Ifng, Il10, Il21, Il21r, Ascl2, Bach2, Batf, Bcl6, Egr2, Elk4, Foxp1, Grhl1, Hmgb2, Irf1, Irf4, Lef1, Maf, Myc, Nfil3, Prdm1, Rbpj, Rora, S1pr1, Stat1, Stat3, Stat4, Tbx21, Tox2, Vdr, Cblb, Entpd1, Nt5e, Serpinb6
795
667
Tet+ vs Tconv hypomethylated
TFH vs Tconv hypomethylated
Hypermethylated region-associated genes
1952
Selplg, Ccr7, Cd28, Icos, Sh2d1a, Tnfrsf18, Ctla4, Havcr2, Ifng, Il21r, Il7r, Tgfbr1, Tgfbr2, Tgfbr3, Bach2, Bcl6, Cbfa2t3, Foxp1, Id2, Id3, Jdp2, Lef1, Maf, Myb, Nfia, S1pr1, Stat1, Tbx21, Tcf7, Tox2, Gzmb, Cblb, Entpd1, Itk
796
452
TFH vs Tconv hypermethylated
Tet+ vs Tconv hypermethylated
C
Distal Intergenic
Gene Body
Promoter
Number of differentially methylated regions
Hypermethylated
Hypomethylated
5000
2500
0
2500
Only in Tet+
Only in TFH
Shared by Tet+ and TFH
Differential status vs. Tconv
D
Hypermethylated (21.7%)
Hypomethylated (78.3%)
Hypermethylated (50%)
Hypomethylated(50%)
Only Tet+ (7%)
Only TFH (5.5%)
Hypomethylated (82.2%)
Hypermethylated (17.8%)
Shared (Tet+ and TFH) (87.5%)
DMRs in Tet+ and/or TFH vs Tconv cells
E
hypermethylated
hypomethylated
log2FC scRNA-seq. TR1/TR1-like vs TFH.1 (scMultiome)
40
20
0
-20
-40
-60
Arhgap15
Bach2
Atxn1
Itga4
Itga4
Il10
Rora
S100a10
Id2
Slamf6
Ptpn22
Jak2
Nrn1
Inpp4b
Ttc39b
Iqgap1
Jmjd1c
Gem
Nfatc1
Rgs16
Il21
Celf2
Odc1
Gna13
Ets1
Maf
Plcb4
Gnaq
Casp4
Fosb
Nfkbiz
Tank
Prkch
Trerf1
Fyn
Nfia
Arid5b
Ptpn13
Cd44
Stat3
Jarid2
Hivep2
Malt1
Slc9a9
Slc9a9
Tnfsf8
Nfkb1
Tox
Only in Tet+
Only in TFH
Shared by Tet+ and TFH
Genes associated with differentially methylated regions found in Tet+ and/or TFH cells relative to Tconv cells (cell type where corresponding gene is differentially methylated)

Figure 4. Gene methylation status in BDC2.5mi/I-A^{g7}-NP-induced Tet+, KLH-DNP-induced TFH and Tconv cells.

(**A**) Venn diagram of differentially methylated regions (DMRs) in BDC2.5mi/I-A^{g7}-NP-induced Tet+ and KLH-DNP-induced TFH vs. Tconv cells. (**B**) Venn diagrams of differentially hypo-methylated (left) or hyper-methylated (right) regions shared by BDC2.5mi/I-A^{g7}-NP-induced Tet+ cells and KLH-DNP-induced TFH cells as compared to their Tconv counterparts. Gene names found in the 106 TFH/TR1/Treg gene list in **Supplementary Table 1**, with shared methylation status, are indicated. (**C**) Bar plot showing the numbers of differentially hypo- or hyper-methylated regions (separated by gene region: promoter, gene body or distal intergenic) in BDC2.5mi/I-A^{g7}-NP-induced Tet+ and KLH-DNP-induced TFH vs Tconv cells, respectively. DMRs are classified, from left to right, into those only found in BDC2.5mi/I-A^{g7}-NP-induced Tet+ cells (Only Tet), KLH-DNP-induced TFH cells (only TFH), or found in both subsets (Shared by tet+ and TFH). (**D**) Pie-donut chart showing the distribution of DMRs (hyper and hypo-methylated status) in genes associated with OCRs (n=328) shared by TFH.1 and TR1/TR1-like cells (identified via scMultiome). (**E**) Jitter plot comparing differential gene expression between TR1/TR1-like and TFH.1 cells (as determined by scMultiome) and differential methylation status, focusing on the genes that remain open at the TR1/TR1-like cell stage, as determined by scMultiome. DMR-associated genes are classified based on their cell pool specificity (i.e. only found in BDC2.5mi/I-A^{g7}-NP-induced Tet+ cells (Only Tet+), KLH-DNP-induced TFH cells (only TFH), or both (Shared by Tet+ and TFH)). Color depicts the methylation status (hypo- or hyper-methylated) of the regions associated with these genes. No significant correlation between methylation status and differential gene expression was found.

Fig. 5


Differential Gene Expression
Differential Methylation
SC Differential OCR
Differential H3K4me3
Differential H3K27me3
Differential H3K27Ac
Intergenic
Gene Body
cds
exon
gap
Gene Body
Promoter
Gene Body
Promoter
Gene Body
Promoter
DE genes inTR1 vs TFH
Ascl4
Otx1
Prdm1
Npas2
Atf3
Klf2
Fosb
Ahr
Tsc22d3
Klf4
Jun
Runx3
Fosl2
Junb
Klf11
Maff
Fos
Pax9
Rara
Csrnp1
Tbx21
Smad7
Irf6
Bach2
Nfil3
Id2
Runx2
Irf4
Taf7
Gm14308
Eomes
Thrb
Taf4b
Thra
Pou2f2
Notch1
Zscan18
Gata1
Cebpa
Bcl6
Nr2f6
Sox8
Pax5
Pbx3
Rora
Hif1a
Gtf2ird1
Pparg
Nfia
Foxm1
Ehf
Tead3
Ikzf4
Maf b
Spic
Spib
Foxp3
Jdp2
Id1
Heyl
E2f7
Hey1
Arnt2
Hlf
Nr4a3
Hif3a
E2f8
Fold Change
2
1
0
-1

Figure 5. **Relative contribution of different epigenetic marks to changes in the expression of differentially expressed TF-coding genes during the TFH to TR1 cell conversion.** Heatmap depicting the presence of different epigenetic marks (from left to right: differential methylation, differential OCRs, differential H3K27ac deposition, differential H3K4me3 deposition and differential H3K27me3 deposition) in BDC2.5mi/I-A^{g7}-NP-induced Tet+ vs KLH-DNP-induced TFH cells. Data correspond to differentially expressed TF-coding genes between TR1 and TFH.1 cells as determined by the scMultiome analyses. Differential epigenetic data is scaled for each technique and when multiple genomic regions are associated to a gene, the average is provided. Genes are arranged from most to least upregulated, followed by least to most downregulated (Fold Change). No differentially enriched sites for H3K27Ac histone deposition were associated with differential expression of these genes.

Fig. 6

A

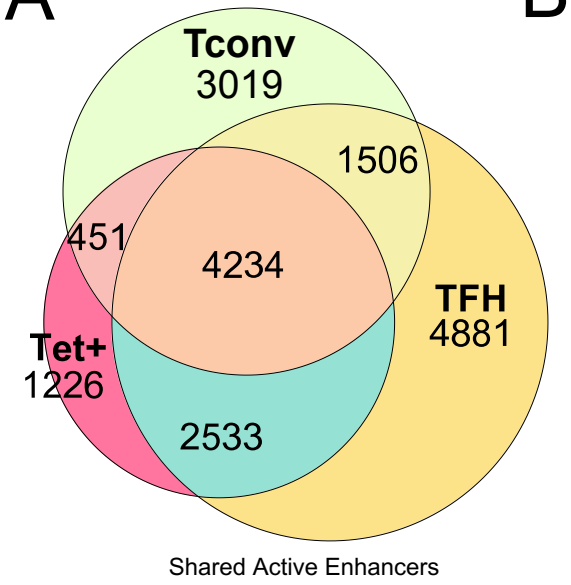

B

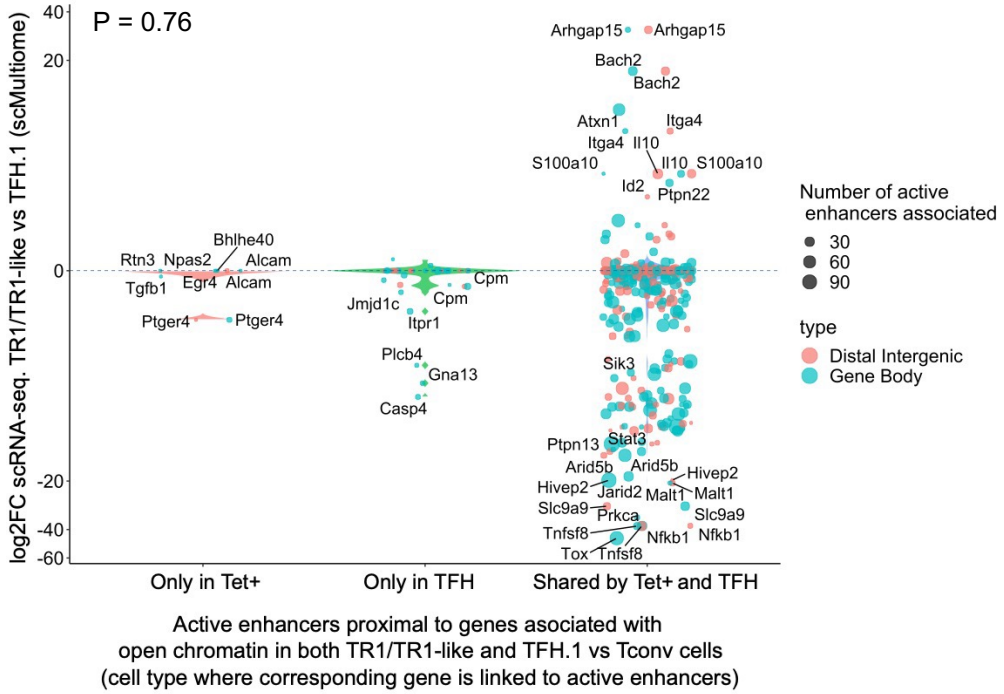

Active enhancers proximal to genes asociated with
open chromatin in both TR1/TR1-like and TFH.1 vs Tconv cells
(cell type where corresponding gene is linked to active enhancers)

C

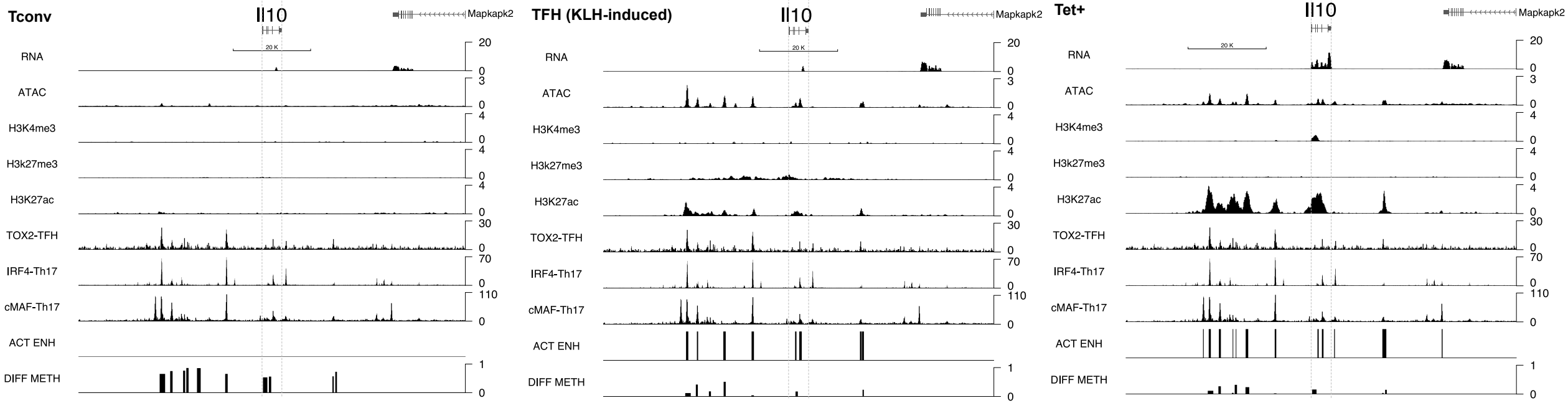

Figure 6. TR1 cells inherit hypomethylated active enhancers from their TFH precursors.

(**A**) Euler's plot showing total active enhancer sharing by BDC2.5mi/I-A^{g7}-NP-induced Tet+ cells, KLH-DNP-induced TFH cells, and Tconv cells. Overlapping of active enhancers in BDC2.5mi/I-A^{g7}-NP-induced Tet+ cells and KLH-DNP-induced TFH cells was significantly higher than overlapping between BDC2.5mi/I-A^{g7}-NP-induced Tet+ and Tconv cells (Pearson's Chi-squared test with Yates' continuity correction P<2.2e-16). (**B**) Jitter plot comparing differential gene expression between TR1/TR1-like and TFH.1 cells (as determined by scMultiome), focusing on the genes that remain open at the TR1/TR1-like cell stage, and both distribution and number of active enhancers per gene as a function of their cell pool specificity (i.e., only found in BDC2.5mi/I-A^{g7}-NP-induced Tet+ cells (Only Tet+), KLH-DNP-induced TFH cells (only TFH), or both (Shared by Tet+ and TFH)). Color and size depict the region type (gene body or intergenic) and the number of active enhancers per gene, respectively. Gene names are displayed for all the genes except when more than 20 dots are in the same region of the plot. No significant correlation between active enhancer distribution and differential gene expression (Wilcox test for differential analysis: adjusted P < 0.05) was found using Pearson's Chi-square test, P = 0.76. **(C) Figure displays g**enome tracks for the various readouts examined herein in Tconv CD4+ T-cells (left), KLH-DNP-induced TFH cells (middle), and BDC2.5mi/I-A^{g7}-NP-induced Tet+ cells (right). Tracks correspond, from top to bottom, to reads for RNAseq (n=4), ATACseq (n=3), ChIPseq (n=1) for H3K4me3, H3K27me3 and H3K4me3 immunoprecipitation, respectively; ChiPseq (n=1) for Tox-2 (TFH cells), Irf4 (Th17 cells), and cMaf (Th17 cells) deposition, respectively (see main text for references), active enhancers and differential methylation, respectively. Visualization reads were normalized to total sequencing depth per sample using BPM (Bins per Million) and, where replicates were available, height mean per bin was also computed. ChIPseq data was also normalized for input (non-immunoprecipitated) sequenced reads. Height (y-axis) is equivalent to the normalized number of mapped reads in each region. Active enhancers (ACT ENH) were predicted as overlapping regions of OCR (ATACseq) and H3K27Ac deposited peaks (ChIPseq

H3K27Ac) and are depicted as absent or present in each region. DIFF METH shows differentially methylated regions (n=3) obtained comparing BDC2.5mi/I-A^{g7}-NP-induced Tet+ cells and KLH-DNP-induced TFH to Tconv cells. Height corresponds to the relative mean methylation value for each region.

Fig. 7

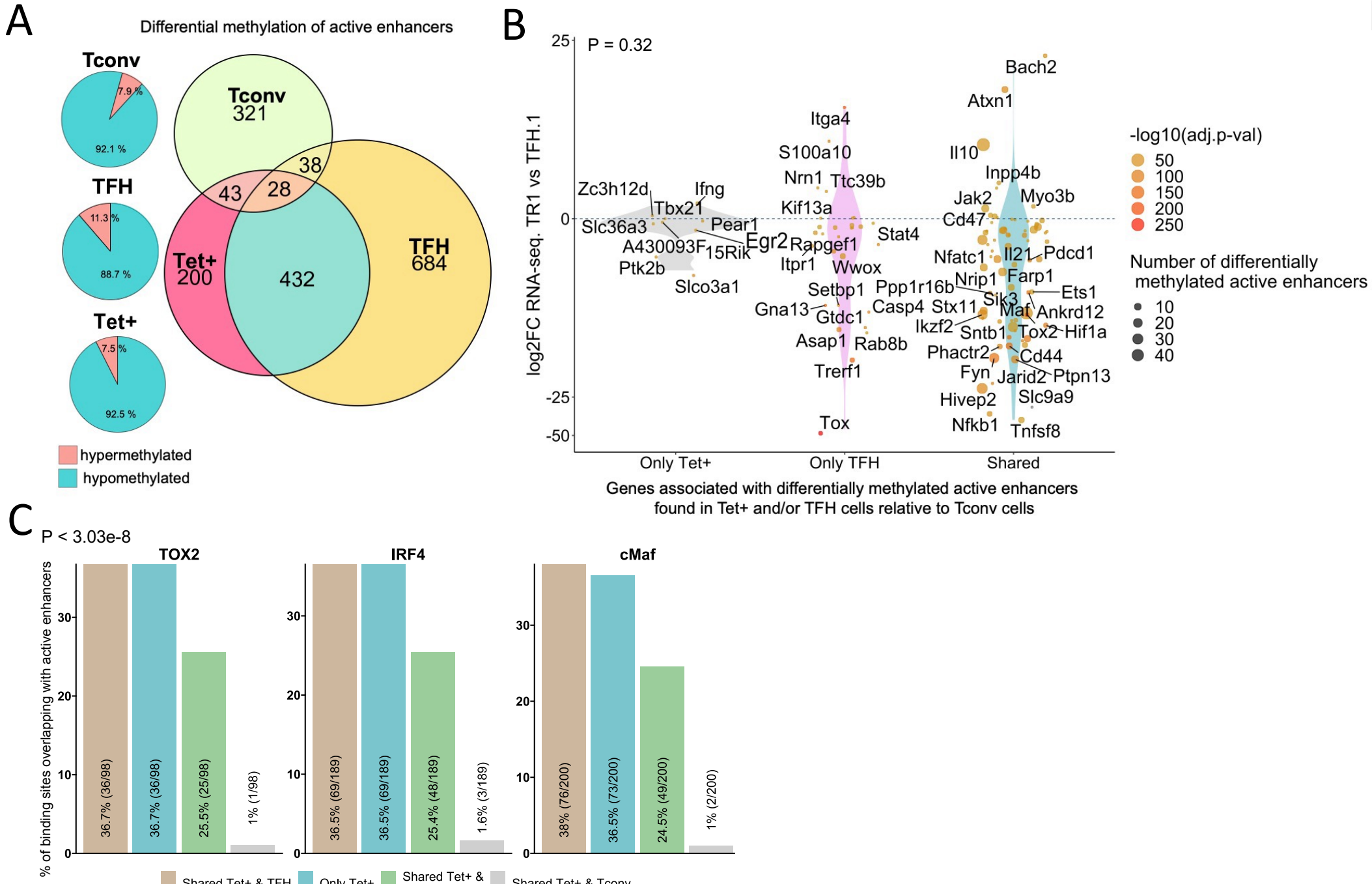
A
Differential methylation of active enhancers
Tconv
7.9 %
92.1 %
TFH
11.3 %
88.7 %
Tet+
7.5 %
92.5 %
Tconv
321
38
43
28
Tet+
200
432
TFH
684
hypermethylated
hypomethylated
B
P = 0.32
log2FC RNA-seq. TR1 vs TFH.1
25
0
-25
-50
Bach2
Atxn1
Itga4
S100a10
Il10
Inpp4b
Nrn1
Ttc39b
Zc3h12d
Ifng
Tbx21
Kif13a
Jak2
Myo3b
Slc36a3
Pear1
Cd47
A430093F15Rik
Egr2
Rapgef1
Stat4
Nfatc1
Il21
Pdcd1
Ptk2b
Itpr1
Wwox
Nrip1
Farp1
Slco3a1
Setbp1
Ppp1r16b
Ets1
Gna13
Gtdc1
Casp4
Stx11
Sik3
Maf
Ankrd12
Ikzf2
Sntb1
Tox2
Hif1a
Asap1
Rab8b
Phactr2
Cd44
Trerf1
Fyn
Jarid2
Ptpn13
Hivep2
Slc9a9
Tox
Nfkb1
Tnfsf8
Only Tet+
Only TFH
Shared
Genes associated with differentially methylated active enhancers
found in Tet+ and/or TFH cells relative to Tconv cells
-log10(adj.p-val)
50
100
150
200
250
Number of differentially
methylated active enhancers
10
20
30
40
C
P < 3.03e-8
TOX2
IRF4
cMaf
% of binding sites overlapping with active enhancers
30
20
10
0
36.7% (36/98)
36.7% (36/98)
25.5% (25/98)
1% (1/98)
36.5% (69/189)
36.5% (69/189)
25.4% (48/189)
1.6% (3/189)
38% (76/200)
36.5% (73/200)
24.5% (49/200)
1% (2/200)
Shared Tet+ & TFH
Only Tet+
Shared Tet+ &
TFH & Tconv
Shared Tet+ & Tconv

Figure 7. Extensive sharing of differentially methylated active enhancers carrying Tox2, IRF4 and/or c-MAF-binding sites in BDC2.5mi/I-A^{g7}-NP-induced Tet+ and KLH-DNP-induced TFH cells vs. Tconv cells.

(**A**) Euler's plots with differentially methylated active enhancers for each comparison: BDC2.5mi/I-A^{g7}-NP-induced Tet+ cells vs Tconv (Tet+; red), KLH-DNP-induced TFH vs Tconv (TFH; orange) and Tconv vs BDC2.5mi/I-A^{g7}-NP-induced Tet+ cells (Tconv; green). Pie charts on the left show the methylation status (hypomethylated or hypermethylated) of each subset of active enhancers for the same subset-to-subset comparisons. The BDC2.5mi/I-A^{g7}-NP-induced Tet+ and KLH-DNP-induced TFH cell subsets share significantly more differentially methylated active enhancers amongst each other than with Tconv cells (Pearson's Chi-squared test with Yates' continuity correction; P < 2.2e-16). (**B**) Jitter plot of differentially methylated active enhancers in BDC2.5mi/I-A^{g7}-NP-induced Tet+ cells (Tet+) and KLH-DNP-induced TFH (TFH) vs Tconv cells vs. differential gene expression along the TFH.1-TR1 axis as determined by scMultiome. Plot corresponds to genes that remain accessible as TFH.1 cells transdifferentiate into TR1/TR1-like cells. The differentially methylated enhancers linked to these genes were classified as being specific for BDC2.5mi/I-A^{g7}-NP-induced Tet+ cells (Only Tet+), exclusive for KLH-DNP-induced TFH cells (Only TFH) or shared by both Tet+ and TFH cells. Gene bubble color depicts -log10 of adjusted P value from scRNAseq differential analysis, and bubble size depicts the number of regions associated per gene. Gene names are displayed for all the genes except when more than 20 dots are in the same region of the plot. No statistically significant associations between the presence of differentially hypo- or hypermethylated active enhancers and gene expression differences were found (Chi-square Test: P = 0.32). (**C**) Overlap of active enhancers with Tox2, IRF4 and c-MAF binding sites**.** Histogram plot compares the relative proportion of the active enhancers linked to genes that are accessible in both TR1/TR1-like and TFH.1 cells (as defined via scMultiome) and that are upregulated in TR1/TR1-like vs TFH.1 cells (as determined via scMultiome), which overlap with binding sites for Tox-2 in TFH cells, and IRF4 or c-MAF in Th17 cells. Bars

correspond from left to right, to: 1) binding sites shared by both BDC2.5mi/I-A^{g7}-NP-induced Tet+ and KLH-DNP-induced TFH cells (Shared Tet+ & TFH); 2) exclusively found in the BDC2.5mi/I-A^{g7}-NP-induced Tet+ pool (Only Tet+); 3) shared by BDC2.5mi/I-A^{g7}-NP-induced Tet+, KLH-DNP-induced TFH and Tconv cells (Shared Tet+ & TFH & Tconv); and 4) shared by BDC2.5mi/I-A^{g7}-NP-induced Tet+ and Tconv cells (Shared Tet+ & Tconv).